UNIVERSITY OF CALIFORNIA SAN DIEGO

A Model on Dendritic Cell Infection by Flaviviruses

A Thesis submitted in partial satisfaction of the requirements

for the degree Master of Science

in

Biology

by

Joan Miquel Valls Cuevas

Committee in charge:

Matthew Daugherty, Chair
Stephen Hedrick, Co-Chair
Barry J. Grant

2020

The Thesis of Joan Miquel Valls Cuevas is approved, and it is acceptable in quality and form for publication on microfilm and electronically:

_____

_____

Co-Chair

_____

Chair

University of California San Diego 2020

EPIGRAPH

My life amounts to no more than one drop in a limitless ocean.
Yet what is any ocean, but a multitude of drops.

David Mitchell

TABLE OF CONTENTS

ABBREVIATIONS

ACR	Adherent cell solution
ADE	Antibody dependent enhancement
BHK	Baby hamster kidney
C	Capsid
cDC	Conventional dendritic cells
CDC	Center for disease control
CMC	Carboxymethyl cellulose
CZS	Congenital Zika Syndrome
DALY	Disability-adjusted life years
DENV	Dengue virus
DC-SIGN	Dendritic Cell-Specific Intercellular adhesion molecule-3-Grabbing Non-Integrin
DF	Dengue fever
DFS	Dengue fever syndrome
DNA	Deoxyribose nucleic acid
DSMZ	Deutsche Sammlung von Mikroorganismen und Zellkulturen
DSS	Dengue Shock Syndrome
E	Envelope
EDTA	Ethylenediaminetetraacetic acid
ER	Endoplasmic reticulum
FACS	Fluorescence-activated cell sorting
FA	Fatty acid
FAS	Fatty acid synthase
FBS	Fetal bovine serum

FcγR	Fragment-crystallizable gamma receptor
FCS	Fetal calf serum
FFA	Focus forming assay
FSC	Forward scatter
GBS	Guillain-Barré syndrome
GM-CSF	Granulocyte-macrophage colony-stimulating factor
HEPES	4-(2-hydroxyethyl)-1-piperazineethanesulfonic acid
HOMER	Hypergeometric Optimization of Motif EnRichment
HFDPC	Human hair follicle dermal papilla cells
FPKM	Fragments per kilobase of transcript per million mapped reads
iDC	Immature dendritic cell
Ig	Immunoglobulin
IL	Interleukin
JEV	Japanese Encephalitis virus
kDa	Kilo Dalton
moDC	Monocyte-derived dendritic cell
MOI	Multiplicity of infection
mDC	Mature dendritic cell
MUTZ-3	Menschliche Und Tierische Zellkulture-3
NBDP	Normal blood donor program
NKV	No known vectors
NS (protein)	Non-structural protein
NTPase	Nucleoside triphosphatase
OCH	Occipitofrontal head circumference

ORF	Open reading frame
PBMC	Peripheral blood mononuclear cells
PCA	Principal Component Analysis
PFA	Paraformaldehyde
PHK	Primary hamster kidney cells
prM/M	Pre-Membrane/Membrane
pDC	Plasmacytoid dendritic cell
qRT-PCR	Quantitative real-time polymerase chain reaction
RIN	RNA integrity number
RNA	Ribonucleic acid
SREBF	Sterol regulatory element-binding factor
SREBP	Sterol regulatory element-binding protein
SSC	Side Scatter
STAR	Spliced transcripts alignment to a reference
TGF	Transforming growth factor
TLR	Toll-like receptor
TNF	Tumor necrosis factor
TSPL	Thymic stromal lymphopoietin
UCSC	University of California, Santa Cruz
UTMB	University of Texas Medical Branch
UTR	Untranslated region
VLDL	Very low-density lipoprotein
WHO	World Health Organization
WNV	West Nile virus

WT	Wild type
YFV	Yellow fever virus
YFV-AVD	Yellow fever vaccine associated viscerotropic disease
ZIKV	Zika virus

LIST OF FIGURES

LIST OF SCHEMA

ACKNOWLEDGEMENTS

I would like to express my deepest gratitude to my mentor Dr. Emilie Branche for providing her time to train me as a proper scientist. Dr. Branche has provided invaluable guidance throughout my Master's program and helped me at inconvenient times. I could not be more thankful for the sacrifices that she made on my behalf and for the growth I have made under her guidance.

I would also like to thank Dr. Sujan Shresta for giving me the opportunity to be in her lab and the opportunity to advance my career while having a small yet meaningful impact in the flavivirus field.

Figures 3-5 are coauthored with Dr. Aaron Carlin. The thesis author was the primary author. Figures 6-7 are coauthored with Dr. Emilie Branche. The thesis author was the primary author.

I would like to acknowledge Dr. Aaron Carlin and Dr. Emilie Branche for allowing me to use figures that they developed for this project.

ABSTRACT OF THE THESIS

A Model on Dendritic Cell Infection by Flaviviruses

by

Joan Miquel Valls Cuevas

Master of Science in Biology

University of California San Diego, 2020

Professor Matthew Daugherty, Chair

Professor Stephen Hedrick, Co-Chair

With an estimated 3.9 billion people at risk of dengue fever, dengue is a major disease threat. Other flaviviruses such as Yellow fever virus (YFV), Japanese encephalitis virus (JEV), Zika virus (ZIKV), West Nile virus (WNV) amongst others, also have a significant burden of disease. For this reason, a model was built that optimizes viral infection in dendritic cells (DCs). DCs are the link between the innate and adaptive immunity and flaviviruses such as DENV, ZIKV YFV, JEV are capable of infecting DCs. Therefore, identifying mechanisms that mediate infection is important to understanding disease progression. We cell sorted populations of infected and

bystander cells and collected RNA of DCs of all these populations. RNA-sequencing (RNA-seq) results indicated that despite similarities in the genome of ZIKV and DENV, they upregulated different pathways. ZIKV upregulated lipid metabolism and DENV upregulated inflammatory pathways when compared against mock. Infection models were similarly created with YFV and JEV vaccine strains. Our infection model, when coupled to a cell sort method provides a powerful method for identifying pro- or anti-viral mechanism from pure infected and uninfected populations.

INTRODUCTION

Over half of the world's population is at risk of flavivirus infection and only two vaccines (YFV and JEV) have been shown to be highly immunogenic. Many of the countries affected by flaviviruses lack the health infrastructure necessary to provide advanced support. While a majority of flavivirus infections can be asymptomatic, infections with symptoms can lead to long-term health issues or death. To reduce the unequal burden of disease, the flavivirus field needs additional knowledge to develop anti-virals and vaccines for other flaviviruses. Studying DCs, one of the first lines of defense and one of the first targets of flavivirus infection, may elucidate how flaviviruses hijack the host machinery to successfully infect humans.

a. Flaviviruses

Flaviviruses evolved from a common ancestor 10 000-20 000 years ago and since then there are many types of flaviviruses that exist (1). For example, flaviviruses can be single or dual host restricted. Single host restricted flaviviruses are restricted to vertebrates and arthropods. In vertebrates these viruses are classified as No Known Vector (NKV). In rodents, NKV viruses include Modoc virus, and, in bats, Rio Bravo virus. Arthropods that transmit flaviviruses include ticks, mosquitos and sandflies. Dual-host tick-transmitted flaviviruses include tick borne encephalitis, Langat and Powassan virus. Many flaviviruses exist; however, of those most well-known, studied, and cause the greatest human impact are insect transmitted flaviviruses. Insect transmitted flaviviruses are dual-host viruses infecting mosquitos, bats, and primates (2). Some of these viruses include West Nile Virus (WNV), Japanese encephalitis virus (JEV), yellow fever virus (YFV),

dengue virus (DENV) and Zika virus (ZIKV) (3). From these viruses, the female *Aedes Aegypti* mosquito is responsible for the spread of YFV, DENV and ZIKV (4).

i. Viral genome organization, coding proteins and morphology

Flaviviruses have a spherical icosahedral shaped envelope formed by envelope (E) protein dimers. They can range between 9 and 13 kilo base pairs (kbs) and are approximately 50 μm in diameter [1][2]. Flavivirus particles contain one viral RNA molecule surrounded by a nucleocapsid composed of capsid (C) proteins which is further surrounded by a lipid membrane [8]. Pre-membrane (prM)/E or membrane (M)/E protein dimers are anchored into this membrane to form the immature or mature viral particles, respectively.

Flavivirus genome is composed of a positive single-stranded RNA approximately 11 000 nucleotides long, varying depending on the virus. Viral genome is composed of a 5' cap but no poly-A tail in 3' and a single open reading frame (ORF) flanked by untranslated regions (UTRs) (5). The ORF serves as a messenger to encode a single polyprotein. Cellular and viral proteases cleave this polyprotein into three structural proteins, capsid (C), pre-membrane/membrane (prM/M) and E proteins, and seven non-structural proteins (NS1, NS2a, NS2b, NS3, NS4a, NS4b and NS5).

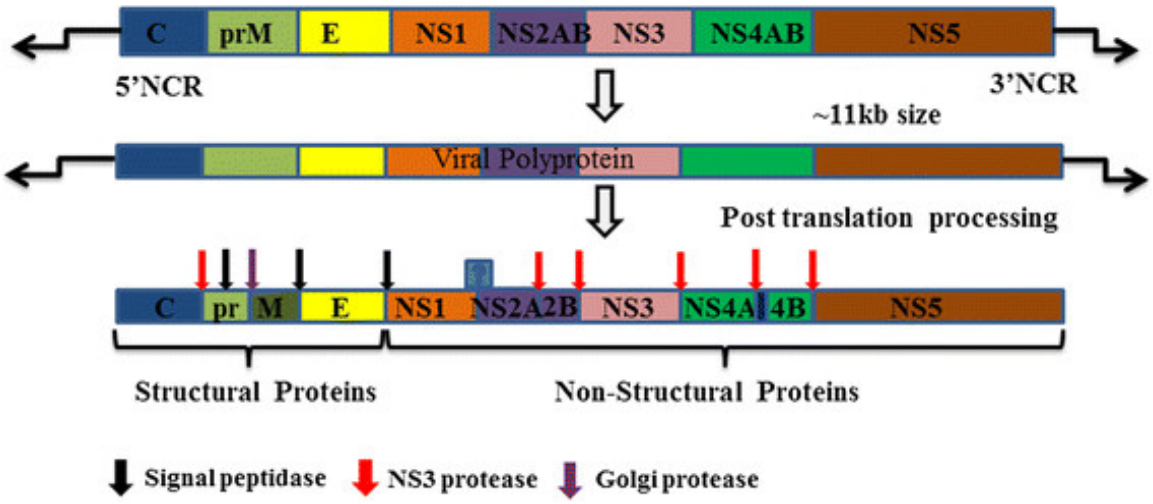

Scheme 1. Overview of flavivirus ORF. Structural proteins and non-structural proteins are shown. Cellular and viral proteases are also shown.
Adapted from Tomar S. *Viral Proteases and their Inhibitors* 2017.

1. Structural proteins

Structural proteins are responsible for the protection of viral RNA and the fusion onto different membranes of the flavivirus life cycle. C protein in flaviviruses is a 14 kDa protein that is responsible for the assembly of the nucleocapsid and lies at the N-terminus of the viral genome. C proteins have an affinity to both nucleic acids and lipid membranes. In this way, C protein can help with nucleic acid rearrangement, promote folding of RNA and simultaneously attach to the lipid membrane (6). C protein is cleaved from the intramembrane signal sequence separating C and prM proteins by NS2B and NS3. prM protein is a 19-21 kDa protein and an integral part of the flavivirus envelope. Furin cleavage prM into M protein results of maturation of the envelope(7). M and E proteins form different types of complexes depending on the stage of viral development. The immature virus is composed of 60 prM/E trimer of heterodimers. After furin cleavage, the mature virus is composed of 90 E protein dimers (8). The E protein of flaviviruses is 53 kDa and is responsible for viral binding and fusion (7) (9). Attachment to cells is mediated by E protein and

promotes the release of the nucleocapsid into the cytoplasm (6). E protein is a main target in the development of humoral immunity (7).

2. Flavivirus Non-Structural proteins

Non-structural proteins are responsible for pivotal viral life-cycle processes and immune evasion. The function of non-structural proteins is often inter-twined and depend on one another. NS1 is thought to be involved in immune evasion and viral RNA processes which occur by interference of the Toll-like receptor (TLR) signaling pathway allowing the virus to replicate with more ease (10). NS3 protein is multifunctional and includes a serine protease, nucleoside triphosphatase (NTPase), and an RNA helicase. Serine protease is responsible for polyprotein cleavage to produce mature viral proteins. NTPase/RNA helicase is involved in RNA replication (10). NS2B is a cofactor used by NS3 for capsid cleavage (7). NS4A is a membrane bound protein implicated in the replication complex and signal sequence to guide NS4B to the endoplasmic reticulum (ER) lumen (11). NS4B is implicated in viral replication by affecting helicase activity of NS3 (11). NS5 protein is a methyltransferase and RNA-dependent RNA polymerase and is responsible for coupling replication and assembly (12).

ii. Flavivirus life cycle

After E protein attachment to cellular factors (including DC-SIGN on dendritic cells (DCs)), flaviviruses enter into human cells via receptor mediated endocytosis and clathrin-mediated endocytosis (13) (14). The endosomal vesicle acidification promotes the fusion of the viral and endosome membranes to release the nucleocapsid and then viral RNA into the cytoplasm. Viral RNA is translated into a single polyprotein by the cellular machinery. This polyprotein is then cleaved by host and viral proteases to obtain structural and non-structural proteins required for the RNA amplification and the replication step. A replication complex is formed by NS2A, NS2B, NS4A and NS4B (11). This replication complex has been theorized to help stabilize the activity of NS3 and NS5, promoting efficient viral production. NS4B traffics the genome to the ER. C protein is cleaved from the intramembrane signal sequence separating C and prM proteins by NS2B and NS3. Immature virus is produced and trafficked to the Golgi. After trafficking immature virus to the Golgi, immature virus is prepared for egress. At this time, a drop in pH and acidic conditions allows cleavage by furin, a cellular protease located in the trans-Golgi network. Furin cleaves prM into M protein(7). However, this cleavage is not 100% efficient; thus, many immature and partially mature viral particles are produced (with no nucleocapsid or genome)(15).

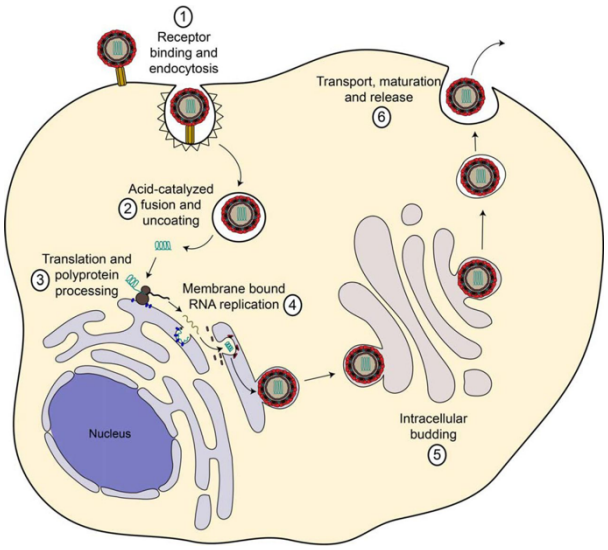

Scheme 2. Overview of Flavivirus life cycle.
Adapted from Gerold G *Molecular and cellular proteonomics* 2017

iii. Dengue

DENV is a flavivirus transmitted by DENV infected female *Aedes Aegypti* or *Aedes albopictus* mosquitos [17]. Four circulating serotypes of DENV exist worldwide (DENV 1-4). Over 50 years after the identification of these four serotypes, a fifth serotype, DENV-5, has been identified. DENV-5 was found after collecting serum from a human patient and responsible for an outbreak in 2007 in the Sarawak state of Malaysia (16).

Dengue-like epidemics were first historically documented in the Caribbean in the 1600's. In 1780, Benjamin Rush described the first dengue-like epidemic with symptoms (Dengue fever syndrome (DF)) in Philadelphia. The disease was described as *break-bone fever* (17). In 1828, in

Cuba, there was a dengue-like due to a virus named Dunga. DENV was first isolated in 1943-1944 by Ren Kimura and Susumu Hotta from infected patient blood in Japan (18).

Before 1970, only 9 countries experienced dengue. In the last 40 years there has been a 30-fold increase in infections (18). Since then, DENV has a become a large burden of disease and over 100 countries are affected (18). As of 2010, it is estimated that 390 million DENV infections occurred and 96 million had clinical manifestations (19). As of 2012, it is estimated that 3.9 billion people are at risk of DENV infection (20). Each year, approximately 500 000 patients require hospitalization and around 12 500 result in fatalities (21).

Different manifestations of DENV infection exist and are characterized by severity, from asymptomatic or mild dengue fever (DF), to severe dengue hemorrhagic fever (DHF) and dengue shock syndrome (DSS). An infected patient can suffer from severe flu-like symptoms such as a high fever and two of the following: severe headaches, pain behind the eyes, nausea, vomiting, swollen glands, muscle and joint pains, and a rash. A second more severe manifestation of DENV known as DHF can by classified if any of the following criteria are present: fever lasting 2-7 days, any hemorrhaging, thrombocytopenia characterized by a platelet count lower than 100 000/mm^3 and increased vascular permeability. If the four criteria are met for DHF and the patient has evidence of circulatory failure, then the patient is diagnosed with DSS. Severe dengue can be fatal due to plasma leakage, fluid accumulation, respiratory distress, severe bleeding, or organ impairment (Mayo clinic, 2018). It is difficult to estimate DENV disease progression. However, one important risk factor known to be implicated in the development of severe dengue is antibody dependent enhancement (ADE).

Despite the large burden of disease that DENV has, only one licensed vaccine, called Dengvaxia, exists against DENV. Dengvaxia was first registered in Mexico in 2015. Mass vaccination (campaign or trial) was performed in the Philippines where 800 000 students were vaccinated. Those patients who had been exposed to dengue before showed protection, however those who had not showed an increased likelihood of developing severe dengue(22). Therapeutic treatments targeting all four serotypes is key to preventing dengue and severe dengue that can be triggered by ADE. ADE can be caused by sub-neutralizing antibodies that bind to FcγRs which increases viral entry and virus production. Cells that express FcγR are susceptible to ADE. Outside of ADE, FcγRs are responsible for many regulatory functions such as: humoral tolerance, modulation of pro- and anti-viral responses, antibody mediated effector functions and cellular immune responses. Many myeloid cells express FcγRs some of which include macrophages, monocytes and mature dendritic cells (mDCs) (23). Patients who have antibodies to one DENV serotype and are later infected by a second serotype may harbor sub-neutralizing antibodies that lead to an increased risk of severe dengue. Similarly, infected infants can be affected by sub-neutralizing antibodies found in breast milk (22). After building an immune response against DENV, antibodies towards a secondary infection with the same serotype over time can be; first neutralizing, then as antibody levels wane over time they can become enhancing and after that can undergo degradation (24, 25). ADE as a result of DENV infection is one of many challenges in producing an effective and safe DENV vaccine.

Sanofi Pasteur designed a vaccine to have protection against all four serotypes. Dengvaxia was created using YFV as a backbone and inserting the E protein of each DENV serotype into a chimeric construct (26). However, current data by Sanofi shows that the vaccine may predispose young children (less than 5 years old) to severe Dengue(22). DENV-3 and DENV-4 had the highest

immunogenicity whereas DENV-1 and DENV-2 had some of the worst results. The inadequate response may lead to an increase in severe cases against DENV-2. As a result, long term cases saw an increase in hospitalizations for DENV-1 and DENV-2. The vaccine also had a higher efficacy in seropositive volunteers compared with naïve seronegative volunteers. Consequently, Dengvaxia has been registered for use in individuals 9 to 45 years old in endemic areas (27).

Outside of vaccine development, different strategies are in the works to tackle DENV. Currently, a monoclonal antibody Ab515 by Visterra binds to domain III of E proteins of all four serotypes and appears to neutralize DENV in target cells(28)[14]. Another approach involves using currently known drug compounds that have already been licensed for use in order to see if there is any effect on viral infection. Through this method, preliminary findings using ivermectin has shown a reduction in serum NS1 levels and body temperature without noticeable viremia levels. ST-148 is a small molecule that targets capsid protein across all four serotypes causing self-interaction. Viral strains that were resistant were detected in the population but selection of a resistant strain under laboratory settings was not observed (6) .

iv. Zika Virus

ZIKV is a flavivirus that can be transmitted by female *Aedes Aegypti, Aedes Albopictus*, and other *Aedes* mosquitos and also sexual fluids. Only one serotype of ZIKV exist with two lineages, the Asian and African lineage. ZIKV was first isolated in 1947 from a sentinel monkey in the Zika forest in Uganda. Prior to the first outbreak of ZIKV, ZIKV was prevalent in mosquitos in Africa and Asia. However, only 13 human cases had been reported (29). The first ZIKV was first reported in the Yap state, one of four states in Micronesia, in 2007. The Yap state has less a population less

than 7 000. After the outbreak, a serosurvey showed that approximately 74% of those tested had IgM antibodies to ZIKV. It is estimated that 72.5% of the population was infected with ZIKV and 18% had a clinical illness (30). In 2013 several islands in French Polynesia began to report outbreaks. The first reported cases and association between ZIKV and Guillain-Barré syndrome (GBS), a neurological condition affecting the peripheral nervous system, was first noticed during this outbreak. In 2014, sporadic ZIKV cases were first reported in Brazil. In 2015 and 2016, a large outbreak occurred in Brazil. In 2015, 1700 cases of GBS were reported(29). After the outbreak, by 2017 there were 217 000 ZIKV cases and 3500 cases of Congenital Zika Syndrome (CZS) reported as a result of the 2015/2016 outbreak in Latin America. In Brazil alone, there were 2300 of CZS cases reported (31) (32).

After infection, 18-35% of cases show signs and symptoms (33). Signs and symptoms of ZIKV include fever, muscle and joint pain that is very similar and nearly indistinguishable from DENV infection. Additional symptoms may lead to a rash or conjunctivitis. More severe complications can include neurological disorders. For example, GBS is possible but rare and accounts for 1.2% of all ZIKV infections(33). Patients with GBS show loss of sensation at the extremities and gradually this progresses up peripheral nervous system. Around 30% of GBS cases can progress to respiratory failure, highlighting the importance of intensive care and management (34). Additionally, it was discovered that ZIKV preferentially infects neural progenitor cells in the developing fetus of pregnant mothers. ZIKV infection in mothers leads to CZS that can be distinguished by microcephaly or the diminished development of the cerebral cortex noted by a reduction in occipitofrontal head circumference (OCH) (35).

The rise of ZIKV infection has caused an economic burden. Congenital syndrome cases in Brazil. Future epidemics in Latin America could cost approximately 2.3 billion dollars per year (32). Since there has been few dengue outbreaks in the continental United States, the possibility of

economic impact of ZIKV was evaluated. It is estimated that medical costs would surpass 1 billion dollars if 1% of the population in Alabama, Florida, Georgia, Louisiana, Mississippi and Texas was affected (36).

v. Japanese Encephalitis Virus

JEV is a flavivirus that is spread by *Culex* mosquitos, primarily *Culex tritaeniorhynchus* (37). Five genotypes of JEV exist that circulate in many parts of Asia. Two of these genotypes are localized to Thailand/Malaysia where JEV is thought to have originated and the other genotypes have expanded their niche to other parts of Asia. JEV is considered a zoonotic virus because humans are dead end hosts. JEV viremia in humans is low enough that JEV is not transmittable between humans and mosquitos cannot be infected by feeding on humans. However, herons, egrets and pigs are viral reservoirs for JEV and replicate to high titers. JEV also grows in mosquito larvae that thrive in rice paddy fields. With birds, there is a potential for JEV to travel around the world and with pigs, due to domestication, perpetuate spread of infection to humans.

JEV was first discovered in the late 19th century in Japan (45). JEV later spread to parts of India in the 1950's and then the rest of India in the 1970's. A large increase in rice production and raising pigs may account for the rapid spread of JEV. Currently, more than 4 billion people are at risk for JEV since JEV affects approximately 25 countries in Asia (37). However, in Japan and North Korea vaccination campaigns and vector control has curbed JEV outbreaks. Regardless, every year it has been estimated that there are 68 000 cases, 20 000 fatal cases and 14 000 to 27 000 cases that result in sequelae (1) (46). Additionally, the global burden of JEV infections account for 700 000 disability-adjusted life years (DALYs) every year (45).

Developing clinical features after JEV infection is not common. Approximately 1-4% of people who are infected develop symptoms. Symptoms can range from flu-like symptoms to fatal encephalitis. Typically, patients show symptoms after 5 to 15 days after initial exposure (37). Of patients who develop encephalitis 20-30% will die as a result of the infection and 30-50% of those who survive will have long-term neurological and cognitive effects (37).

The first JEV vaccine, JE-VAX, was produced by infecting young mice intracerebrally and inactivating the brain homogenate supernatant with formalin. However, JE-VAX was not cost-effective and also had adverse effects and in rare instances caused a serious allergic reaction or neurological complications. JE-VAX production has stopped being produced in favor of other safer and cheaper vaccines. Another JEV vaccine, SA14-14-2, was licensed in China in 1988 and was grown in primary hamster kidney (PHK) cells (37). SA14-14-2 was produced from the infectious S14 strain and is highly immunogenic with a single dose.

vi. Yellow Fever Virus

YFV is a flavivirus in the Flaviviridae family that is transmitted by mosquitos. YFV is mainly transmitted by female *Aedes Aegypti* mosquitos in the urban sylvatic cycle. In the jungle sylvatic cycle such as in the jungles of Africa, YFV can be transmitted by *Aedes africanus*. However, this mode of infection is very infrequent since the *Aedes africanus* feeds at night and does not prefer to bite humans (26). YFV can also be transmitted by mosquitos in the genera *Haemagogus* and *Sabethes*. In southern Brazil, *Haemagogus* and *Sabethes* are the primary genera that spread YFV in the jungle sylvatic cycle (38). YFV originated in the jungles of Africa and was imported to the

Americas during the slave trade. YFV is endemic in the Americas and Africa co-circulating with other flaviviruses but has remained clear of Asia where other flaviviruses are circulating(26). The Asibi strain was first isolated from a patient in 1927 and is still in use. From this strain, a live-attenuated vaccine strain called YFV17D was developed through serial passaging in nervous-tissue deprived embryo of chicks (26) (39) . After more than 150 passages, YFV was found to not infect when injected intracranially.

There are three phases to YFV infection: the acute, remission and toxic phase. The incubation period lasts 3 to 4 days and many people do not experience symptoms. However, those that do can experience fever, backache, headache, loss of appetite, nausea or vomiting. During the remission stage, symptoms typically subside after 3 to 4 days from the initial infection. Approximately 15-20% of patients enter the third phase, the toxic phase. This can occur within 24 hours or as late of 48 hours of recovering from initial symptoms (26). During the toxic phase, symptoms include: a high fever, gastrointestinal hemorrhage, and jaundice dysfunction can occur in organs such as the liver, kidneys or cardiovascular. In deceased patients, pathology reveals enlargement of these organs. At this late stage, viremia is absent, but antibodies can be detected (26).

YFV17D live-attenuated vaccine strain is effective because it has retained the ability to replicate and induce an immune response through a persistent viral infection, where RNA, neutralizing antibodies and a T-cell response has been detected weeks after infection (40) (41). Even though a vaccine exists, YFV still has a significant impact in Africa and South America where there are 200 000 infections and 30 000 deaths annually (26). On the other hand, YFV vaccination in 2016 averted approximately 94 000 to 119 000 cases in endemic zones (42).

YFV17D live attenuated vaccines was regarded as one of the safest vaccines. However, a report published in 2001 found an association of vaccine induced infection to YFV which caused

severe hemorrhagic disease. The report highlighted 7 cases, 6 being fatal, of Yellow fever vaccine associated viscerotropic disease (YFV-AVD). Approximately 0.4 in 100 000 in the US were found to develop YFV-AVD which fortunately is very rare (40). The vaccine can provoke an attack on the liver, kidneys or the nervous system. In areas where YFV is endemic there are about 0.24 cases for every 100 000 people vaccinated as a result of the vaccine (43). It is estimated that 1 in every 7 infections is apparent with the wild-type (WT) strain and with the vaccine strain it is 1 in every 250 000 (44). Due to YFV-AVD the WHO has recommended people that only people that live in or plan to travel to endemic countries are vaccinated against YFV. Despite the development of YFV vaccine, little is known about how long-lasting immunity is induced with the vaccine. Therefore, studying the immune reaction of cells infected by YFV may elucidate pathways implicated in the building of a long-lasting immunity.

b. Dendritic cells

Dendritic cells (DCs) are a main target of DENV and can be infected by ZIKV, YFV and JEV(47) (48) (41). DCs are produced from hematopoietic stem cells in the bone marrow with two distinct origins: a myeloid origin such as that of phagocytes involved in immunity, and a lymphoid lineage of T-cells, involved in regulation and tolerance (49). Within the myeloid origin, two main subsets of DCs exist, conventional (cDCs) and plasmacytoid DCs (pDC). cDCs can uptake and process both extra- and intracellular antigens. These antigens are then presented to either CD8+ T-cells by (cDC1), or to CD4+ cells by (cDC2) (50). pDCs can sense intracellular DNA and RNA of virus or self through TLR7, TLR9 and are specialized to produce IFN-α (50) (51).

DCs capture antigens and migrate to lymphoid tissues. Under the steady state, marked by no infection or inflammation, DCs can exist in immature or semi-mature states. Immature DCs reside in the skin or mucosal surfaces and therefore are one of the first cells to interact with pathogens (52). After interacting with pathogens, DCs activate B or T-cells to trigger the adaptive immune system. When DCs recognize antigens and they have a strong stimulus, they undergo maturation (49). DC maturation connects the innate and adaptive immune system as different stimuli can lead to differentiation of T-cells towards different outcomes. CD40L and thymic stromal lymphopoietin (TSPL) are two different stimuli that drive DC differentiation. Naïve T-cells differentiate into either Th1 due to CD40L DCs or Th2 cells due to TSPL DCs (49).

In the following study, two possible models to study infection were utilized, human primary monocyte derived dendritic cells (moDCs) or cell line (MUTZ-3)

i. moDCs

The first model type of dendritic cells is moDCs. The CD1 family of which CD1a is a part of, is responsible for antigen presentation in dendritic cells (53). In the presence of granulocyte-macrophage colony-stimulating factor (GM-CSF) and Interleukin-4 (IL-4), monocytes differentiate into immature DCs (iDCs) and a high percentage of these cells express CD1a (53). In the presence of GM-CSF and IL-4 monocytes show a decrease in CD14, a monocyte marker, expression after differentiation. Immature moDCs express high amounts of Dendritic Cell-Specific Intercellular adhesion molecule-3-Grabbing Non-Integrin (DC-SIGN) or CD209. DENV uses DC-SIGN to attach to DCs to facilitate viral entry that is found in iDCs (23).

ii. MUTZ-3

The second model explored was a CD34+ stem cell lineage leukemia cell line. Cell lines allow us to reduce human donor variability between experiments. Unlike primary cells which do not divide, cell lines are also able to be continuously cultured and expanded until they are ready to be used. Therefore, we investigated the potential of MUTZ-3 to function as a cell line. MUTZ-3 cell line was created after isolating blood from a patient with acute myelomonocytic leukemia. MUTZ-3 cell line is amongst one of the best candidates for a DC-like human cell line (54). However, CD34+ stem cells derived DCs are phylogenetically distant to moDCs(55). Regardless, this cell lines shows morphological and phenological characteristics of monocytes. Amongst various cells lines studied, MUTZ-3 has the capability to be differentiated into DC-like cells with the addition of cytokines as indicated by upregulation of CD1a and downregulation of CD14. Kosten et al. report twenty percent CD1a expression after addition of GM-CSF, transforming growth factor- β (TGF-β) and IL-4 for the production of Langerhans-like cells (56). After addition of GM-CSF, IL-4 and a low dose of TNFα, 20% of cells expressed CD1a (57). Santegoets et al. report 60% to 90% of these cells show expression of CD1a similarly using GM-CSF, IL-4 and TNFα (54).

In this report, PBMCs from were isolated from human blood samples in order to isolate monocytes and differentiate them into moDCs. A model was built to optimize infection time and

multiplicity of infection (MOI) or the ratio of viral particles to cells for infectious viruses DENV-2, ZIKV, and vaccine strains JEV SA14-14-2 and YFV17D. For DENV-2 and ZIKV, MOI 1 and MOI 0.5 for 24 hours resulted in about 50% bystander and infected cells. RNA was collected from mock cells. RNA was also from both by-stander non-infected and infected cells after cell sorting from this mixed population. RNA transcriptional profile of all three populations was studied using next-generation sequencing. For YFV17D, the model generated mixed results where some experiments showed no infection and others showed some infection. However, JEV consistently showed infection of DCs. MUTZ-3 cell line was used as an alternative to moDCs and were differentiated however no infection was observed.

MATERIALS AND METHODS

Key reagents, Abs etc. used in this study are outlined in Appendix.

Mosquito cell C6/36 (Ae. Albopictus)

C6/36 cells were purchased from ATCC. C6/36 cells were grown in L15 media supplemented with 10% Fetal Bovine serum (FBS), 100 U/mL penicillin, 100 µg/mL streptomycin and 10 mM HEPES. Media was exchanged every 3 to 4 days in a T175 non-vented flask containing 25 mL of media and 1.0 x 10^6 cells. Cells were passed and expanded when confluency was 80-100%. Cells were scraped from T175 flasks using a cell scraper and collected onto a conical tube. Cells were spun at 1200 rpm for 5 minutes at 4˚C. Cells were resuspended and plated at 28˚C.

Vero E6 cells

African green monkey kidney-derived Vero E6 cells were purchased from ATCC. Vero cells were maintained in DMEM supplemented with 10% FBS, 100 U/mL penicillin, 100 µg/mL streptomycin and 10 mM HEPES buffer. Cells were plated onto a T175 flask and media was changed every three to four days or when confluency reached 80-100%. In order to re-plate cells, cells were lifted using 0.25% Trypsin-EDTA for 2 minutes at 37˚C.

MUTZ-3 cells

Cells were obtained from the Leibniz institute, German collection of microorganisms and cell cultures (DSMZ). Cells were grown in MEMα media containing 20% FBS, 100 U/mL penicillin, 100 U/mL streptomycin and 40 ng/mL of GM-CSF. Cells were seeded at 7.0 x 10^5 per well in 24 well plates, media was exchanged every 5 days. Cells were differentiated using 150 ng/mL of GM-CSF and 50 ng/mL of IL-4. Cells were also differentiated using 150 ng/ml GM-CSF and 50 ng/ml IL-4 or 100 ng/mL GM-CSF, 20 ng/mL IL-4 and 2.5 ng/mL TNFα.

Baby Hamster Kidney (BHK-21) cells

BHK-21 cells were purchased from ATCC. BHK-21 cells were grown in MEMα media containing 10 mM HEPES buffer, 100 U/mL penicillin, 100 µg/mL streptomycin and 10% heat-inactivated FBS or fetal calf serum (FCS). When cells were approximately 80% confluent, cells were passaged. BHK-21 cells were collected and flask was washed with 10-15 mL of 1x PBS applied to the side of a T-175 flask. PBS was aspirated and 2 mL of adherent cell solution (ACR: 1x PBS, 5mM EDTA, 10mM HEPES buffer, 100 U/mL penicillin, 100 µg/mL streptomycin) was added. The ACR was incubated with the cells for 2 minutes at 37˚C to lift the attached BHK-21 cells. Cells were lifted and 10 mL of BHK media was added. BHK-21 cells were centrifuged at 1200 rpm for 5-10 minutes, resuspended, and plated.

Viruses

DENV UIS 353 strain serotype 2 (DENV-2) was used to perform experiments. The virus is a clinical isolate collected in 2004 in Bucaramanga Santander, Colombia from acute sera of an infected patient. The virus was passaged three times in C6/36 cells before arriving to our lab. DENV-2 arrived to our lab in February 2018 and was grown in mosquito cells to produce a working stock.

ZIKV SD001 is a clinical isolate collected from blood or serum 3 days post infection from a patient that had recently returned from a trip to Venezuela in March 2016. SD001 was grown in C6/36 cells for 13 days and virus was ultra-centrifuged.

YFV17D virus was obtained from the Sette lab at La Jolla Institute. YFV17D full length was produced via electroporation onto Vero cells and collected 4 days post-electroporation on August 28, 2012. The virus was passaged once to produce a P1 stock in 2012 and a second time in 2019 to produce virus used in the experiments outlined in this report. The virus was grown in C6/36 to create a stock and similarly in Vero cells.

JEV SA14-14-2 was isolated in 1954 from *Culex pipiens* mosquitos. The virus was isolated in Shan'Xi, China. The virus was acquired by University of Texas Medical Branch (UTMB) in 2008 and lyophilized to ship to the Shresta lab in February, 2019. Lyophilized JEV was grown in Vero cells to produce a P1 stock and grown again in Vero cells to produce a working stock (P2).

Virus prep

Once cells (C6/36 or Vero) reach 80% confluency, cells are ready for infection. Media was aspirated and replaced with media containing no FBS. Media with no FBS was combined with 100 µL aliquot of virus to infect the cells. Cells were infected for 2 hours, rocking flask every 15 minutes. C6/36 cells were incubated at 28˚C in a non-vented T-175 flask. Vero cells were incubated at 37˚C in 5% CO_2 in a vented T-175 flask. Infectious media was removed and replaced with fresh media containing 10% FBS. Cells were collected and concentrated at the first sign of cytopathic effect. Virus containing media was collected and for JEV no concentration of virus was performed. JEV SA14-14-2was collected at day 4 and day 5 post infection.

Concentration of virus

Media containing virus was collected at the first sign of cytopathic effect and centrifuged for 15 minutes at 2500 rpm at 4˚C in order to remove cellular debris. An Amicon column was washed using 15 mL of molecular grade biology water and centrifuged for 10 minutes at 2500 rpm, a 50K column was used to concentrate YFV17D and a 100K column was used for DENV-2. Flow-through was dumped and virus-containing media was added to the top of the filter on the Amicon tube. Tube was centrifuged at 2 800 g for 15 to 20 minutes depending on final volume. Ideally a volume of 0.5 to 2 mL of concentrate is desired in the column. Concentrate left on the column was collected and supernatant that had flown through was discarded. Centrifugation was repeated, adding virus containing media to the top of the column. With the same column, this step can be repeated up to four times. Concentrate was filtered through a 0.22 µm filter to ensure sterility. Virus was aliquoted and stored at -80˚C. ZIKV was ultra-centrifuged at day 13. For ultra-centrifugation virus was spun

at 28 000 rpm for 90 minutes at 4˚C. Supernatant was discarded and virus was resuspended in 300 µL of 20% FBS in 1x PBS.

Quantification of viral titer by focus forming Assay (FFA)

BHK-21 cells were plated at 2.0 x10^5 cells /well in a 24 well plate and incubated overnight at 37°C using BHK media. Ten-fold virus dilutions are performed from no dilution until 10^{-11}. To infect the BHK-21 cells, 100µL of virus or diluted virus was placed onto each corresponding well in BHK media. Plate was rocked every 15 minutes at 37°C in 5% CO_2 for 2 hours. In order to avoid the spread of virus, 1 mL of prewarmed BHK media containing 1% carboxymethyl cellulose (CMC) was added. Wells were incubated at 37˚C in 5% CO_2 for 2.5 days for JEV and DENV-2, and 3 days for YFV17D and ZIKV.

Cells were fixed 2.5 or 3 days after infection with 1 mL 4% formalin diluted in 1x PBS and incubated for 30 minutes at room temperature. Supernatant was removed by dumping and wells were washed three times with 1x PBS. In order to permeabilize the cell membrane, 500 µL of 1% Triton™X-100 in 1x PBS was added and incubated for 20 minutes at room temperature and washed using 1x PBS. In order to block non-specific binding, 500 µL of 10% FBS diluted in 1x PBS and incubated for 1 hour at room temperature. Blocking solution was removed but no washing was performed. Primary stain was performed using 400 µL of 4G2 (1 µg/mL) diluted in PBS/1%FBS and incubated 1 hour at room temperature. Plates were washed three times with 1x PBS after incubation. Secondary staining was performed using anti-mouse IgG HRPO ab (JACKSON) at 1:1000 in 1x PBS and 1% BSA for 1.5 hours at room temperature. Plate were washed three times with 1x PBS. In order to visualize foci present, 200 µL of True Blue™ peroxidase was added to each well. After a 20-30

minutes incubation in True Blue™ plate was washed once using deionized water to remove excess True blue. Plates were dried and placed away from direct light using aluminum foil at room temperature. Foci were counted the following day.

PBMC isolation

Blood from healthy donors from the Normal Blood Donor Program (NBDP) at LJI were used in the experiment. After the phlebotomy lab drew blood from patients, blood was prepared for PBMC isolation. Cold Histopaque®-1077 was added to a propylene tube. For 100 mL of blood or more collected from a donor 50 mL of 1x PBS and 0.02% EDTA was added. Blood/PBS/EDTA mixture was gently added to the tube containing Histopaque®-1077 while avoiding mixing of both solutions. The tube was centrifuged at 400 g for 30 minutes at 4°C and ramp and brake were set to 1. After centrifugation, the second layer from the top was collected. The second layer from the top is characterized by a buffy coat. Most of the plasma layer was aspirated off, while not disturbing the top layer. Plasma, buffy coat and Histopaque®-1077 layers were pipetted into a new tube and fill with 0.02% EDTA in 1x PBS. Solution was centrifuged at 300 g for 10 minutes at 4°C with ramp acceleration and deceleration set to 5. Remaining blood cells were lysed using 4.5 mL of molecular biological grade water and 500 µL of 10x PBS was added immediately and mixed with a pipette. Sample was passed through a 70-100 µm filter to remove lipids.

Monocyte isolation

Human monocyte cells were isolated using magnetic labeling and separation through negative selection with MACS Miltenyi biotech kit. First, PBMCs were counted using the Vi-CELL

XR cell counter. The lymphocyte protocol was used and a 1:10 dilution using 1x PBS to determine the quantity of reagents to use. PBMCs were spun at 300 g for 10 minutes and resuspend using 30 µL of MACS Buffer (0.5% BSA in Auto macs rinse solution) for every 1.0 x 10^7 PBMCs. For every 1.0 x 10^7 PBMCs 10 µL of FcR blocking reagent was added and mixed and similarly the same amount of Biotin-antibody cocktail was added and incubated for 10 minutes at 4°C. After incubation, for every 1.0 x 10^7 PBMCs, 30 µL of MACS buffer was added and mixed and 20 µL of Anti-Biotin microbeads were added and incubated for 10 minutes at 4°C.

One pre-separation filter was placed on top of a LS column. The column was placed in the grove of the magnetic separator and securely fitted. The filter and LS column were rinsed with 3 mL of MACS buffer and flow-through was discarded. Cell suspension was added to the column and flow-through was collected. In order to fully rinse the column, 3 mL of MACS buffer was added to the column and flow-through was collected. The entire volume was allowed to flow-through before repeating the next wash. A total of three washes were performed. Flow-through was collected into one tube, spun down at 300 g for 10 minutes and resuspended. Cells were counted using the ViCell XR cell counter by diluting cell suspension 1:10 in 1x PBS. Monocytes were resuspended to 1.5 x 10^6 cells/mL.

Monocyte differentiation in DC

Isolated monocytes were grown in RPMI1640 + Glutamax media supplemented with 10% FBS, 100 U/mL penicillin, 100 U/mL streptomycin and 25 mM HEPES. Cells were seeded at 1.5 x 10^6 cells/mL with 3 mL in 6-well plates. Monocytes were differentiated into monocyte-derived DCs

(moDCs) by adding 100 ng/mL GM-CSF and 100 ng/mL IL-4 for 7 days. No differentiated control cells were not given GM-CSF and IL-4. Fresh media containing (for differentiated cells) or not containing cytokines was exchanged at day 3, and day 6.

Differentiation confirmation

At day 5-7 of differentiation, differentiated cells were collected and spun down at 1500 rpm for 10 minutes. Cells were resuspended, counted, and further diluted to 1.0 x 10^6 cells/mL. Differentiated and undifferentiated samples were plated (1.0 x 10^5 cells) onto a 96-well plate. Cells were stained with 1:100 APC-CD1a and FITC-CD14 conjugated antibodies in FACS buffer for 20 minutes at 4˚C, unstained samples were incubated in 100 µL of FACS buffer. BD LSRII-3 was used for FACS analyses using the Diva acquisition software. In order to confirm differentiation, percent extracellular expression of CD1a and CD14 of cells was quantified. moDCs were utilized for infection when the percent of cells which express CD1a was greater than 70%, otherwise the cells were discarded.

siRNA treatment using reverse transfection

At day 6 of differentiation, cells collected and spun at 300 g at 4˚C for 10 minutes. Cells were resuspended at 1.5 x10^6/mL in DC media with 100 ng/mL GM-CSF and 100 ng/mL IL-4. Cells were transfected with no siRNA or siRNA for control, fatty acid synthase (FAS), sterol regulatory element-binding factor 1 (SREBF1) or SREBF2. Solution was incubated at room temperature for 20 minutes. The solution was placed on an empty 6-well plate and 1 mL of cell suspension was added directly on top of the reagent solution without pipetting up and down. Plate was rocked to ensure that

the media covered the entire bottom of the plate. Plate was incubated at 37˚C in 5% CO_2 for 4 hours and 2 mL of DC media containing 100 ng/mL GM-CSF and 100 ng/mL IL-4 was added to each well. Wells were incubated for different time points (24, 48, 72 hours). After the incubation time, cell and supernatant was collected. Wells were washed with 1 mL of 1x PBS and solution was spun at 12 000 rpm at 4˚C for 5 minutes. Media was aspirated and cells were washed using 1 mL of 1x PBS. Cells were spun at 12 000 rpm at 4˚C for 5 minutes. Solution was aspirated and cells were lysed in 300 µL of RNA lysis buffer. Samples were stored at -80˚C.

RNA isolation after siRNA transfection

RNA was isolated according to the manufacturer's instructions using Quick-RNA micro prep kit. A 1:1 volume of 100% absolute ethanol and sample was prepared and pipetted up and down to ensure that proper mixing. A small precipitate may form, and this is important to keep. Solution was added onto an IC column from Quick-RNA micro prep kit. Sample was spun at 13 000 g for 30 seconds. DNA digestion buffer was prepared in an RNase free tube using 5 µL of DNase I and 35 µL DNA digestion buffer per sample, mixture was mixed by inversion. In order to wash the column, 400 µL of RNA wash buffer was added to the column to prewash column. Column was centrifuged at 13 000 g for 30 seconds. Sample was incubated at room temperature for 20 minutes after adding 40 µL of DNase reaction mix. Flow-through was discarded and 400 µL of RNA prep buffer was added to the column and spun for 30 seconds at 13 000 g. Flow-through was discarded and 700 µL of RNA wash buffer to the column and centrifuged at 13 000 g for 30 seconds. Flow-through was discarded and 400 µL of RNA wash buffer was added to column. Column was centrifuged at 13 000 g for 2 minutes to ensure removal of wash buffer. Column was transferred onto an RNase-free tube and 15 µL of DNase/RNase-free water was added. Column was incubated for 1-2 minutes at room

temperature and spun at 13 000 g for 30 seconds. RNA was diluted to 100 ng/µL using molecular grade water and stored at -80˚C or used directly for cDNA synthesis step.

cDNA synthesis and qRT-PCR

The following cDNA synthesis master mix was prepared: 0.5 µL of iSCRIPT enzyme, 2 µL of 5x iSCRIPT buffer and 7.5 µL of sample RNA at diluted to 100 ng/µL. The mix was placed into PCR tubes and the PCR machine was ran with the following settings: 5 minutes at 25˚C, 20 minutes at 46˚C, 1 minute at 95˚C, and 4˚C until sample was removed.

cDNA was then used for the qRT-PCR. A 1:4 dilution was performed on cDNA samples by adding molecular grade water. The following master mix was prepared: 5 µL of iTaq DNA polymerase 0.5 µL of reverse primer, 0.5 µL of forward primer, 4 µL of diluted cDNA. The following settings were used for qRT-PCR: 94˚C for 2 minutes, 40 cycles of 94˚C for 15 seconds followed by 60˚C for 1 minute, and optional hold at 4˚C. Forward and reverse primers used were obtained from IDT DNA. Primer sequences are listed in the supplementary list of reagents.

Viral Infection

Wells containing moDCs were infected with virus mixed with DC media for 2 hours. Virus-free DC media was used for mock group. During this 2-hour infection the wells containing the minimal volume to cover the well was used in order to increase the contact between cells and virus. Plates were rocked every 15 minutes to ensure even spread of virus. After a 2-hour infection period, cells were collected and centrifuged at 200 g for 10 minutes. Media was aspirated and cells were

washed once with 1x PBS and centrifuged at 200 g for 10 minutes in order to remove excess extracellular virus present. Cells were plated on a new plate.

For experiments involving optimal timepoint or MOI determination, cells were collected at the determined time point (as mentioned in the figure/legend). Time points tested were (6, 12, 18, 24, and 48 hours) throughout some or all experiments. At the indicated time point, supernatant was collected for experiments such as for FFA. Cells were washed with 1x PBS and centrifuged at 200 g for 10 minutes. Cells were resuspended with 200 µL of FACS buffer.

Cellular Staining

Differentiation verification staining

In order to assess differentiation of dendritic cells, differentiated and undifferentiated cells were stained with CD1a-APC and CD14-FITC at 1:100 for 20 minutes at 4˚C placed away from light. Unstained samples were prepared as a control. Sample conditions that have both an unstained and stained group were resuspended in 400 µL of FACS buffer. Stained and unstained samples received equal volumes, 200 µL.

Viral infection percent determination

Extracellular staining was performed using CD1a-APC at 1:100 in FACS buffer for 20 minutes at 4˚C away from light. After cell fixation, intracellular staining of moDCs was performed using 4G2-FITC at 1:100 in perm wash for 30 minutes at 4˚C away from light.

Cell sorting Staining

Dead cells were stained using Zombie Violet™ diluted 1:1000 in 1x PBS and samples were incubated for 20 minutes at 4˚C away from light.

Data analysis

Using Flojo, gating of cells was performed by gating live cells based on the side scatter (SSC) and forward scatter (FSC). Gating was also performed for CD1a-APC by using unstained moDCs as a negative control. CD1a+ cells were used in order to gate for 4G2-FITC.

Cell sort preparation and staining for RNA sequencing

After Zombie violet staining, cells were washed with FACS buffer and samples were spun at 300 g for 5 minutes at 4˚C in order to quench dye with excess protein. Supernatant was removed and samples were resuspended in 1x PBS. Sample was spun at 300 g for 5 minutes at 4˚C. Samples were permeabilized with 1x PBS, 4% paraformaldehyde (PFA), 0.1% saponin and 400 U/mL of RNase inhibitor. Samples were centrifuged at 1000 g for 3 minutes at 4˚C and wash buffer containing 0.2% BSA, 0.1% saponin and 400 U/mL of RNase inhibitor resuspended in 1x PBS. Human Fc block was added at 1:100 in staining buffer containing 1% BSA, 0.1% saponin, 1:25 RNase inhibitor resuspended in 1x PBS. Fc block was incubated for 5 minutes at 4˚C and 4G2-AF647 at 1:100 was added. Stain was incubated for 30 minutes at 4˚C. Cells were centrifuged at 1000 g for 3 minutes at 4˚C and supernatant was removed. Cells were washed twice using wash buffer containing 0.2% BSA, 0.1%, and 400 U/mL of RNase inhibitor resuspended in 1x PBS and spun at 1000 g for 3 minutes at 4˚C. Supernatant was removed and samples were resuspended in sort buffer containing 0.5% BSA and 1600 U/mL of RNase inhibitor resuspended in 1x PBS.

After this sample preparation, the mixed population of cells infected and uninfected cells residing in the same sample was sorted by the LJI flow core using the FACS Aria machine. Zombie

Violet positive cells were excluded from cell sorting and 4G2 positive and negative cells were placed on separate tubes.

RNA isolation for cell sorting

Directly after cell sorting RNA was isolated using total nucleic acid isolation kit following the manufacture's instruction. Digestion buffer master mix was prepared with RNA inhibitor at 400 U/mL and protease solution at 1:50. Sorted samples were spun at 5000 rpm at 4˚C and centrifugation was repeated until all the sample was centrifuged. Master mix was added to sorted fixed-cell samples and incubated at 50°C for 3 hours. After incubation, samples were stored at -80°C or RNA isolated.

Isolation additive solution was prepared using 240 µL of isolation additive and 550 µL of 100% ethanol for each sample. Master mix was added to samples and 700 µL of sample/ethanol mixture was placed onto a column containing a filter cartridge. Column was centrifuged at 10 000 rpm for 60 seconds. Flow-through was discarded by aspiration under a sterile biosafety cabinet. Steps were repeated until all sample/master-mix had been used. In order to rinse the column, 700 µL of wash buffer 1 was added to filter column. Sample was centrifuged, flow-through was discarded via aspiration and wash 2/3 was added. Sample was centrifuged and flow-through was discarded via aspiration and centrifuged an additional 60 seconds.

DNA digestion master mix was prepared using 50 µL of nuclease-free water, 6 µL of 10x DNase buffer and 4 µL of DNase per sample. Samples were incubated for 30 minutes at room temperature using the DNA digestion master mix and 700 µL of wash 1 buffer was added to each filter column. Samples were incubated for 60 seconds and centrifuged at 10 000 rpm. Solution was discarded via aspiration and wash buffer 2/3 was added to the filter column and repeated a second time. Sample was centrifuged for 1 minute at 10 000 rpm to remove residual fluid. Filter cartridge

was transferred to a new column and 50 µL of TE buffer was added to solubilize and protect the RNA. Sample was incubated at room temperature for 1 minute and column was centrifuged at 13 200 rpm for 1 minute. RNA concentration and purity were determined using the nanodrop. Samples were stored at -80°C for long term storage. The Bioanalyzer was used in order to determine the RNA integrity number (RIN) of the samples. Sample was used for RNA-sequencing when the RIN value was above 8.

RNA-Seq and Data analysis

Pre-processing of data was performed by mapping FASTQC files to the University of California, Santa Cruz (UCSC) genome build hg38 (human). The algorithm Spliced Transcripts Alignment to a Reference (STAR) was used to map RNA-seq experiments using default parameters. Hypergeometric Optimization of Motif EnRichment (HOMER) was used to map uniquely aligned reads into tag directories.

RNA-seq reads were aligned to GRCh38/hg38 genome. RNA-seq reads aligned to the GRCh38/hg38 assembly were used to generate gene expression fragments per kilobase of transcript per million mapped reads (FPKM) values using HOMER. Genes with less than 0.5 FPKM in all conditions were defined as not expressed. HOMER's analyseRepeats.pl utility was used to quantify reads in transcript exons defined by GENCODE. Differentially expressed genes and regularized log (r-log) normalization values were calculated using Bioconductor's DESeq2 function. Enrichment values (logP) were clustered using cluster 3.0. Principal component Analysis (PCA) was performed in R.

RESULTS

a. moDCs are sufficiently differentiated

DCs are known to be an important target during flavivirus infection (23). To determine the impact of flavivirus infection on DCs, we wanted first to develop a DC model. Monocytes isolated from human PBMCs were differentiated into moDCs using 100 ng/mL of GM-CSF and IL-4. Figure 1A shows percent of cells expressing CD14, a specific monocyte marker. Over 90% of non-differentiated cells (no cytokines added) show CD14 expression whereas differentiated cells (cytokines added) show less than 10% CD14 expression. Figure 1B similarly shows CD1a (specific dendritic cell marker) percent expressing cells. Less than 10% of differentiated cells show CD1a expression whereas over 80% of differentiated cells show expression of CD1a. These results suggest that monocytes were differentiated into moDCs.

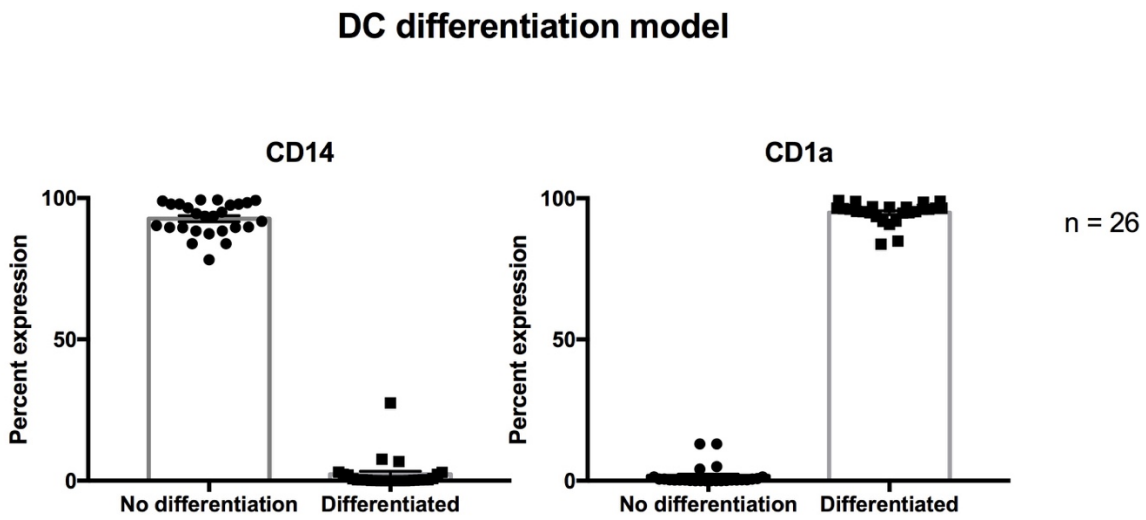

Figure 1. Differentiation verification of monocytes. Cells were stained with CD1a-APC and CD14-FITC on day 7 of incubation in 100 ng/mL of GM-CSF and IL-4. Each value represents one experiment conducted. Mean (± SEM) was plotted for (n = 26).

b. moDC-Flavivirus infectious models established for some but not all flaviviruses studied

Once the DC model was established, to investigate how flavivirus infection impacts DCs, we wanted to develop a DC infectious model. Therefore, we assessed the conditions (MOI and timepoint) necessary to have an ideal infection. Intracellular virus present was quantified by measuring 4G2-FITC via flow cytometry ((Figure 2A, 2C, 2E and 2G). Extracellular viral particles were determined by FFA using BHK-21 cells (Figure 2B, 2D, 2F).

Intracellular infection with DENV-2 (MOI 1), ZIKV (MOI 0.5) and JEV (MOI 1) peaked at 24 hours post infection, at ~40%, ~50% and ~20% of cells infected respectively (Figure 2A, 2C and 2E). Extracellular infectious particles increased over time and plateaued at ~1 x 10^5 FFU/mL at 48 hours (Figure 2B). Intracellular infection with ZIKV peaked at of cells infected at 24 hours post infection (Figure 2C). Extracellular virus increased over time and plateaued at ~1 x 10^6 FFU/mL at 48 hours (Figure 2D). Intracellular infection with JEV SA14-14-2 peaked at ~20% of cells infected at 24 hours post infection (Figure 2E). Extracellular virus increased over time and plateaued at ~1 x 10^5 FFU/mL at 48 hours (Figure 2D).

Figure 2E shows intracellular infection with YFV17D (MOI 1). No cell infection was observed for 3 donors assessed. However, infection was observed for two donors. For one donor, infection peaked at ~6% at both 6 and 12 hours post infection. For the second one, infection peaked at ~20% at both 6 and 12 hours post infection.

We successfully show that DCs are infected after DENV, ZIKV, and JEV infection and optimized infection conditions (MOI and time point) in order to cell sort for RNA sequencing.

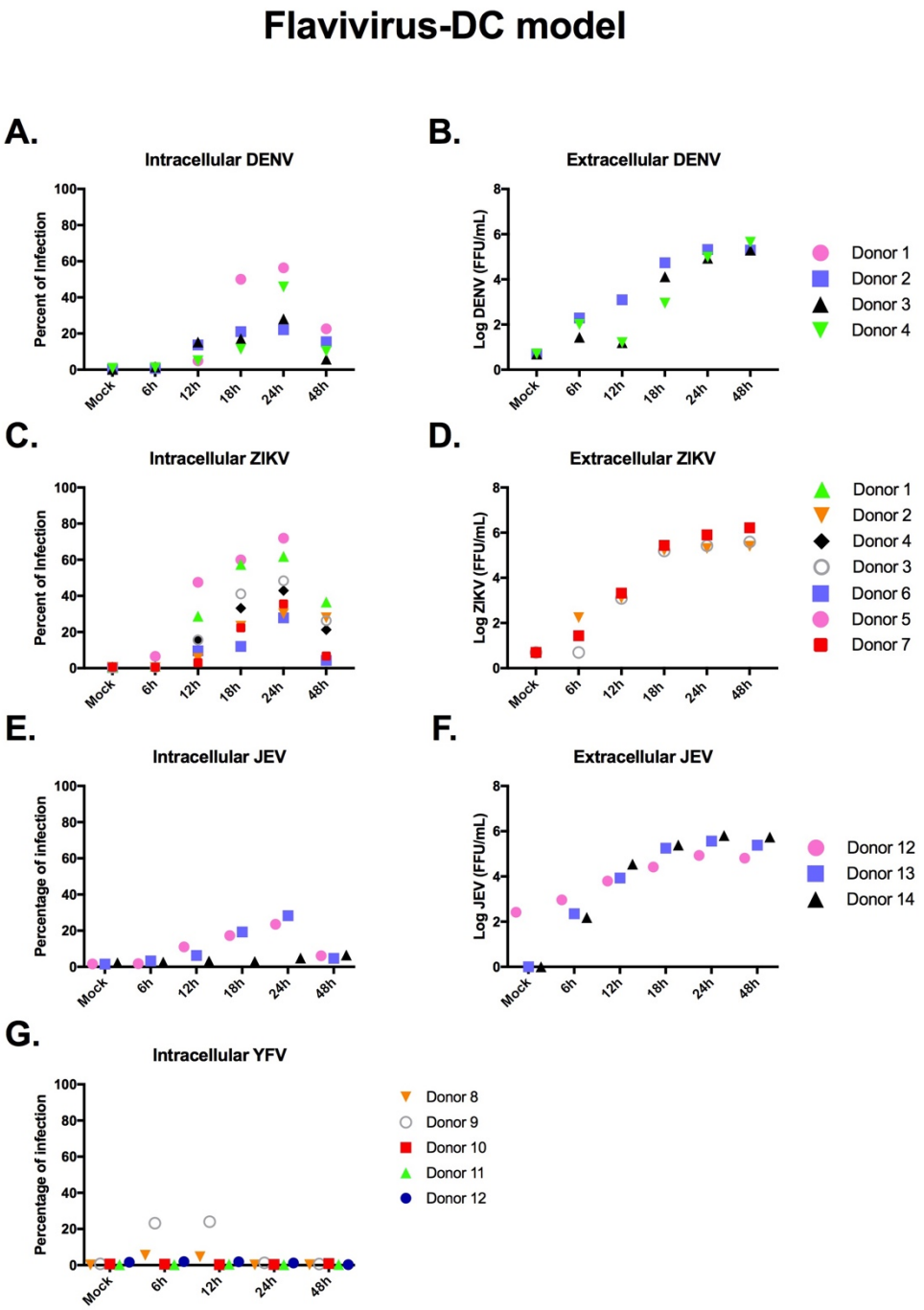

Figure 2. Flavivirus-DC infectious model. moDCs were infected for 6h, 12h, 18h, 24h and, 48h. Percent of cells infected (cells expressing 4G2) by (A) DENV-2 (MOI 1), (C) ZIKV (MOI 0.5), (E) JEV SA14-14-2 (MOI 1), and (G) YFV17D (MOI 1) were quantified by flow cytometry (n=4, n=7, n=3 and n=5 respectively). Extracellular infectious (B) DENV, (D) ZIKV, (F) JEV SA14-14-2 particles production were determined by FFA (n=3).

c. ZIKV and DENV infection utilize different pathways

To study specific pathways that are necessary or pivotal to flavivirus survival and spread. After DCs and infectious models were established, we used a human macrophages model already develop in our laboratory but updated for moDCs (58). This model allowed us to study the modifications induced by the flavivirus infection in a pure population of infected moDCs (Figure 3).

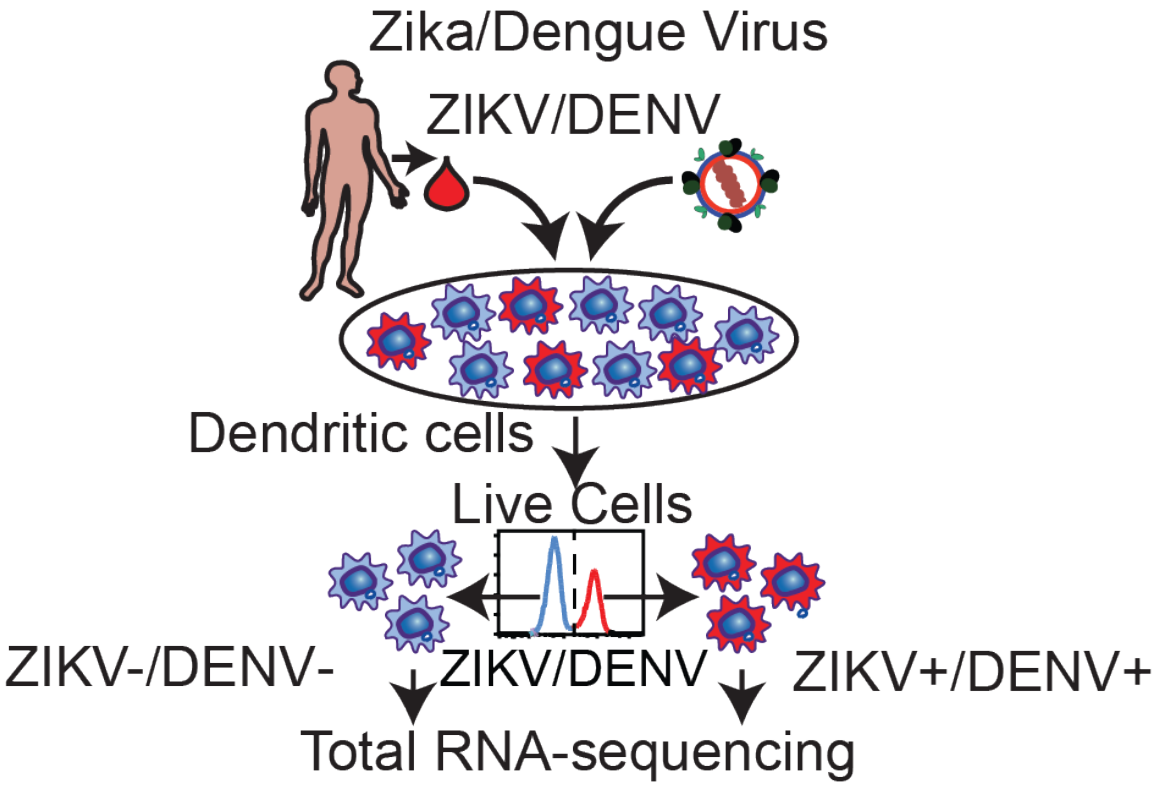

Figure 3. Flavivirus-DC infection model for RNA-sequencing.
moDCs were infected with ZIKV (MOI 0.5) or DENV (MOI 1) for 24 hours. Live cells were sorted into negative bystander cells (ZIKV- or DENV-) or positive infected cells (ZIKV+ or DENV+). Using these populations, RNA isolation was conducted in order to perform RNA-sequencing.

After obtaining results from RNA sequencing, one method of confirming that our RNA sequencing was effective was to produce a PCA plot. Samples within the same group clustered together in the PCA plot. Uninfected bystander cell and infected cell RNA samples clustered

separately along the PC1 axis representing 36% of the variability in the data. DENV and ZIKV samples clustered separately along the PC2 axis representing 24% of the variability in the data, Figure 4. First, this suggests that our sequencing results were relevant and then that ZIKV and DENV have distinct and unique transcriptional effects on moDCs. Infected and bystander cells similarly have distinct impacts on moDCs.

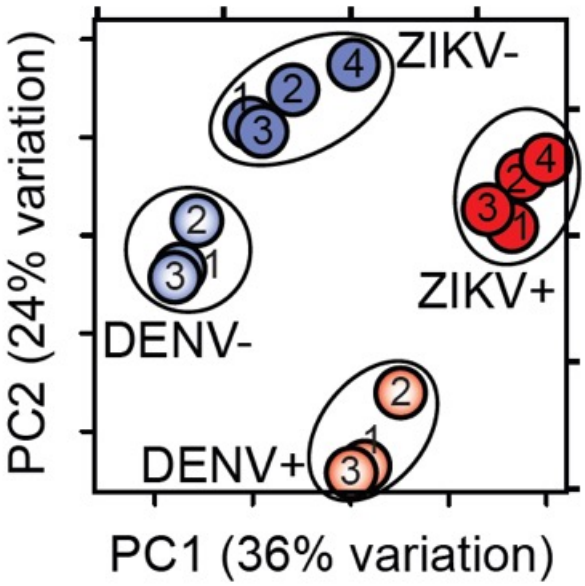

Figure 4. PCA results show clustering of samples. Principal component (PC1) and PC2 were plotted for both DENV and ZIKV and uninfected bystander samples and infected samples. Gene expression for mock samples was used as a baseline and subtracted from uninfected bystander and infected samples. Three of the same donors were used for both DENV (n = 3) and ZIKV (n = 4).

Genes that were upregulated as a result of viral infection were studied. For ZIKV and DENV, genes that were upregulated in infected samples compared to mock was quantified for Figure 5. Results show 347 and 144 upregulated genes when compared against mock in DENV and ZIKV infection respectively. The top 20 pathways related to the upregulated genes were listed. Percent of genes upregulated in the pathway was quantified using different size of circles. After ZIKV infection, pathways in lipid and metabolic metabolism were upregulated. After DENV infection, pathways

related to inflammation and cytokine signaling were upregulated. The amount of upregulation as noted using Log_{10}(q-values) was represented by color. These results suggest that despite ZIKV and DENV being genetically similar, infection leads to different outcomes.

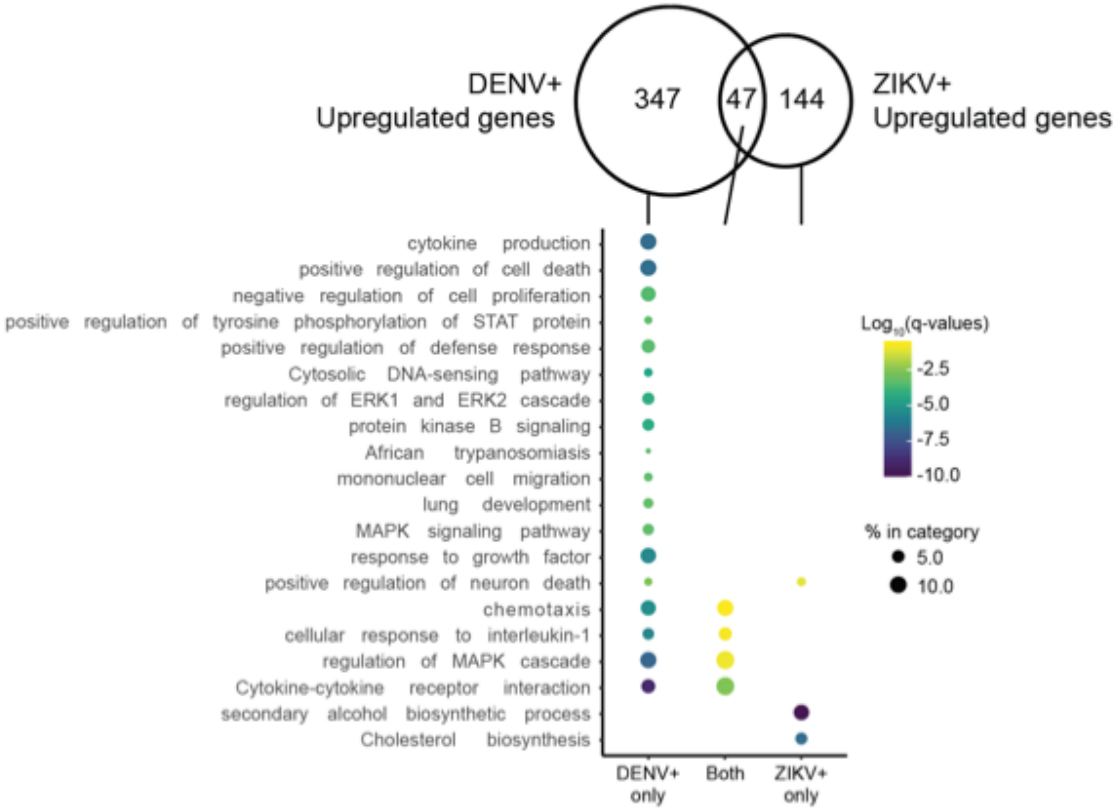

Figure 5. RNA sequence result summary of data. Venn Diagrams showing upregulated genes in ZIKA and DENV infected cells. Top twenty pathways of moDCs after flavivirus infection are shown for both viruses and the overlap of both. Significance is plotted by Log_{10}(q-values). Percent of upregulated genes in gene ontology categories are displayed by the size of the circle.

d. siRNA experiments

In order to study the main pathways upregulated during ZIKV infection in moDCs, we silenced 3 key proteins implicated in lipid metabolism using siRNA. Two transcription factors silenced, SREBP1 encoded by SREBF1 and SREPB2 encoded by SREBF2, are implicated in fatty acid (FA) and cholesterol pathways respectively. fatty acid synthase (FAS) is also implicated in fatty acid pathways and is a limiting enzyme implicated in FA neosynthesis.

siRNA for SREBF1 transfection mixture was prepared for 25, 50, 75 and 150 pmol, Figure 6. Treatment of moDCs with siSREBF1 at 25 pmol shows a ~70% decrease in mRNA across all three time points (24h, 48h and 72h) (Figure 6A). Treatment of moDCs with siSREBF1 at 50 pmol shows a ~85% decrease in mRNA at 24 hours post treatment and ~50% decrease in mRNA at 48 and 72 hours post treatment (Figure 6B). Treatment of moDCs with siSREBF1 at 75 pmol shows a ~65% decrease in mRNA levels at all three time points (Figure 6C). Treatment of moDCs with siSREBF1 at 150 pmol shows a ~65% decrease in mRNA levels (Figure 6D). The data suggests that applying 25 pmol siSREBF1 treatment at 24 hours is sufficient to knockdown mRNA sufficiently and that increasing treatment concentration or time is not significant to further reducing gene expression. A western blot of protein of interest will determine the appropriate concentration of siRNA to use.

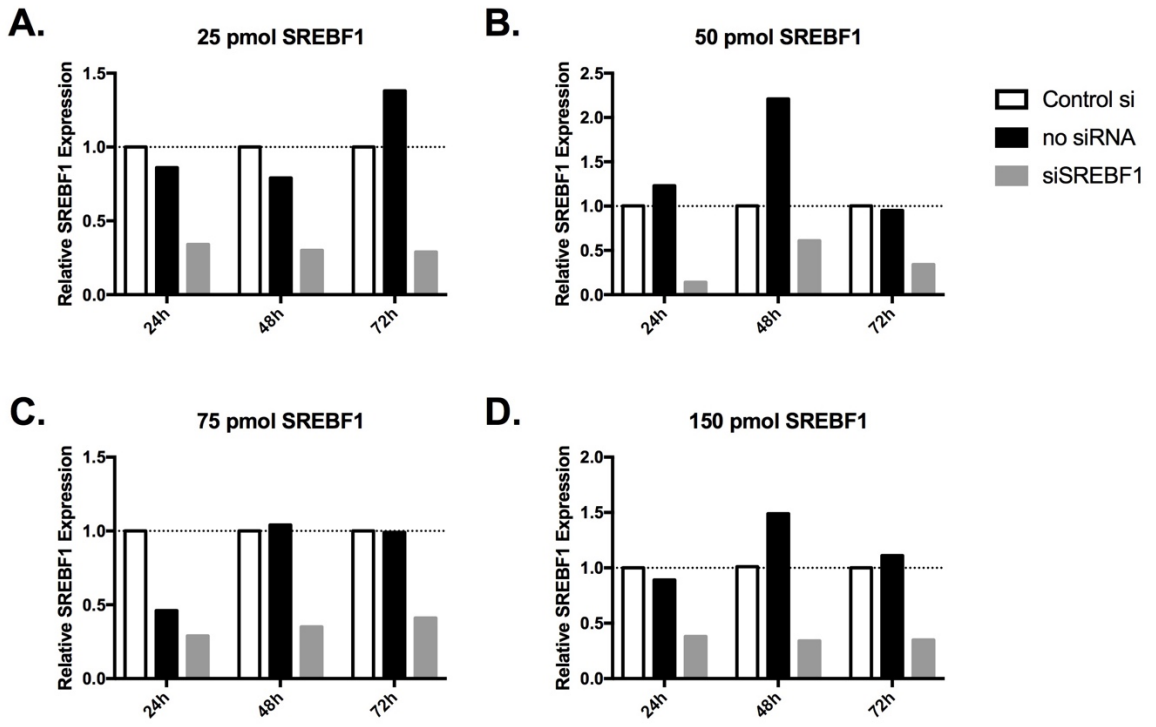

Figure 6. siSREBF1 inhibits SREBF1 across different time points and siRNA concentrations. qRT-PCR results from moDCs after SREBF1 inhibition at different concentrations of siRNA. Increasing concentrations of siRNA were used, 25, 50, 75, 150 pmol (A-D). Relative expression is plotted against control siRNA.

After sufficiently knocking down SREBF1 with siRNA, we sought to knockdown SREBF2 and FAS genes. Treatment of moDCs with siFAS at 25 pmol shows a ~60% decrease in mRNA levels (Figure 7A). Treatment of moDCs with siFAS at 50 pmol shows a ~72% decrease in mRNA levels (Figure 7B). Treatment of moDCs with siFAS at 25 pmol shows a ~66% decrease in mRNA levels (Figure 7C). Treatment of moDCs with siFAS at 50 pmol shows a ~78% decrease in mRNA levels (Figure 7D). The data suggests that applying 25 pmol siSREBF2 or siFAS treatment at 24 hours is sufficient to knockdown mRNA sufficiently and that increasing treatment concentration or time is not significant to further reducing gene expression.

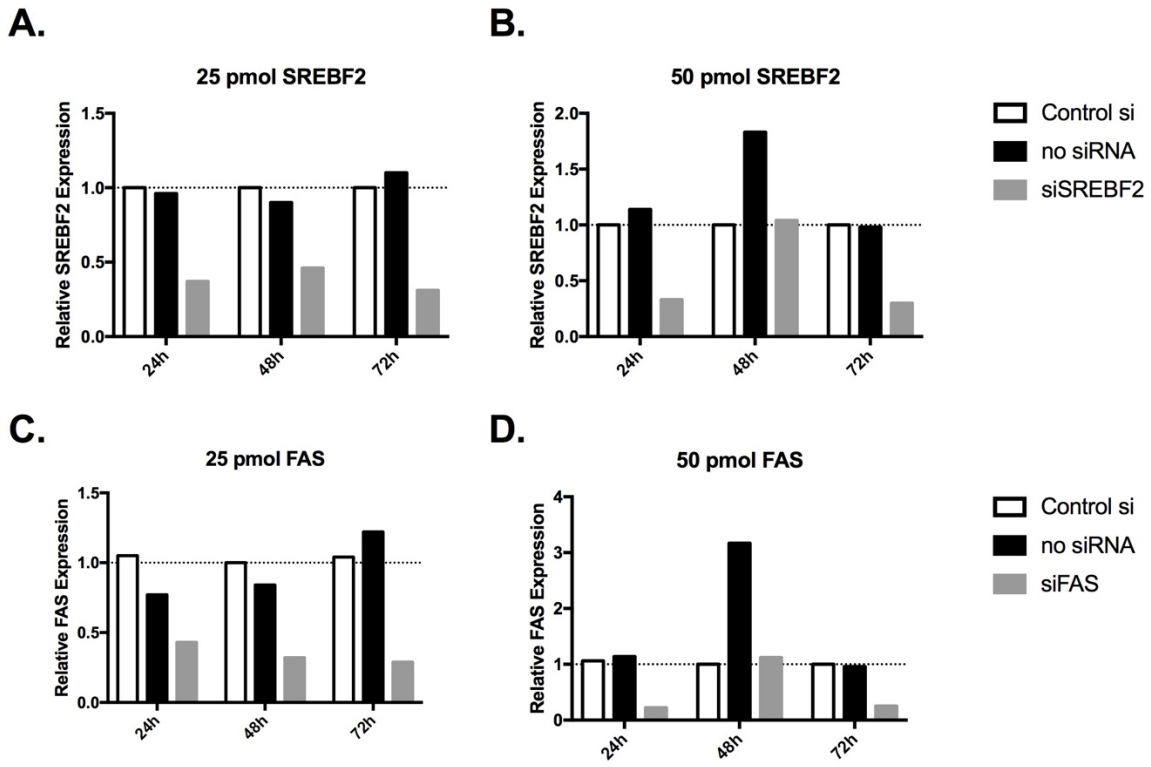

Figure 7. SREBF2 and FAS are silenced across siRNA concentrations and timepoints. qRT-PCR results from moDCs after inhibition with siRNA. Two siRNA amounts, 25 pmol (A and C) and 50 pmol (B and D) show silencing of both SREBF2 and FAS using siRNA across three time points relative to control siRNA.

e. MUTZ-3 model, a monocytic cell line, was differentiated but not infected by ZIKV

To reduce donor variability between experiments and to perform experiments that cannot be conducted easily in primary cells, we wanted to develop an alternative DC cell line model. We assessed he potential of MUTZ-3 cells. This cell line has been shown to display morphologic and phenotypic characteristics of *in vitro* DCs after differentiation with cytokines (57). Therefore, we explored MUTZ-3 cell line as a candidate for our DC-flavivirus infection model. We used two differentiation protocols to differentiate MUTZ-3 in immature DC-like cells. Our first protocol is composed of 150 ng/mL of GM-CSF and 50 ng/mL of IL-4 while our second protocol is composed of 100 ng/mL of GM-CSF, 20 ng/mL IL-4, 2.5 ng/mL TNFα. Using the first protocol, CD14 was significantly downregulated from 24% in not differentiated cells to 13% in differentiated cells and

similarly CD1a expression was significantly upregulated from 10% of MUTZ-3 cells expressing CD1a (cytokines not added) to 50% of MUTZ-3 cells (cytokines added) (Figure 8A). Using the second protocol, MUTZ-3 cells that were differentiated showed a percent decrease of cells expressing CD14 from 20% (no cytokines added) to nearly 0% (cytokines added) (Figure 8C). An increase of MUTZ-3 cells expressing CD1a+ from 10% (no cytokines added) to approximately 85% (cytokines added) (Figure 8D). In this cell model, cells are considered differentiated if CD1a expression is above 20% (59). Therefore, these results suggest that the second protocol allows for a better differentiation, however, the first protocol is sufficient in promoting differentiation.

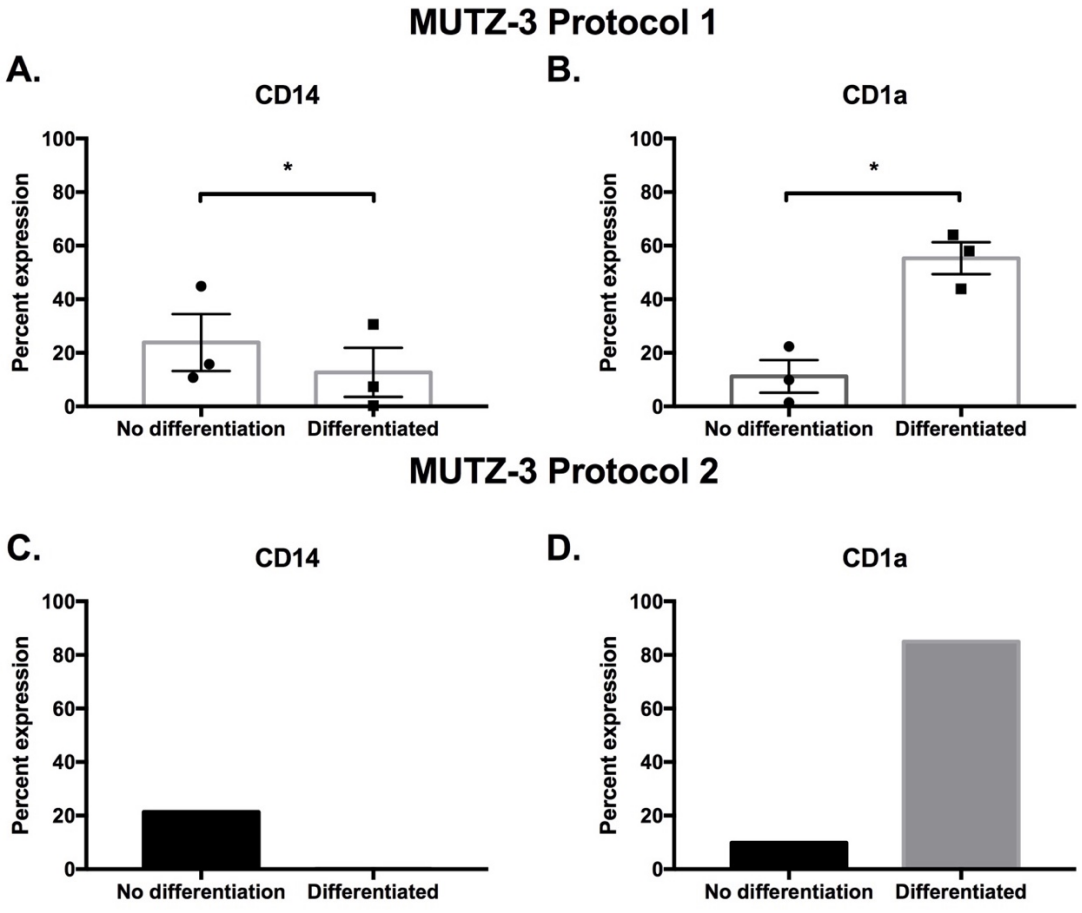

Figure 8. MUTZ-3 differentiation model using two different cytokine protocols. (A and B) MUTZ-3 cells were differentiated using cytokines, 150 ng/mL of GM-CSF and 50 ng/mL of IL-4 for seven days or grown cytokine-free (not differentiated). (A) MUTZ-3 cells expressing CD14 was plotted for cytokine-free cells and cells with cytokines, using protocol 1. (B) MUTZ-3 cells expressing CD1a

was plotted for cytokine-free cells and cells with cytokines, using protocol 1. Mean (± SEM) was plotted for CD14 and CD1a expression, n = 3. (C and D) MUTZ-3 cells were differentiated using cytokines, 100 ng/mL of GM-CSF, 20 ng/mL of IL-4, and 2.5 ng/mL TNFα, for seven days (n = 1). (C) MUTZ-3 cells expressing CD14 was plotted for cytokine-free cells and cells with cytokines, using protocol 2. (D) MUTZ-3 cells expressing CD1a was plotted for cytokine-free cells and cells with cytokines, using protocol 2. Mean (± SEM) was plotted for (n = 3). A paired two-tailed t-test ($p < 0.05$).

f. MUTZ-3 cells are an inadequate infection model

Using the two differentiation protocols, MUTZ-3 cells were infected with ZIKV. Cells infected with ZIKV (24, 48 hours and MOI 0.1, 0.5, 1) were stained with 4G2-FITC in order to determine the percent of infected MUTZ-3 cells. Figure 9 shows percent of CD1a+ cells that express intracellular 4G2 using either the first (Figure 9A) or the second (Figure 9B) differentiation protocol. Results indicate that across all time points (24h and 48h) and MOI (0.1, 0.5 and 1) percent of cells expressing 4G2 was 0% or nearly 0% for all three experiments. This suggests that even though MUTZ-3 cell line was able to become adequately differentiated, this is not sufficient for ZIKV infection.

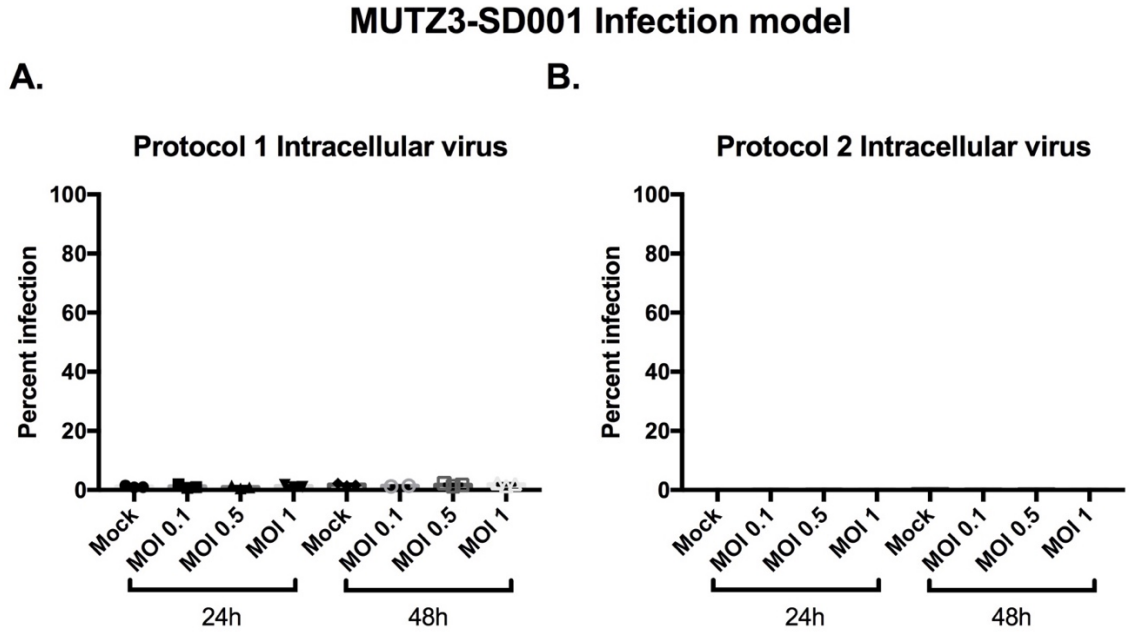

Figure 9. MUTZ-3 Infection with ZIKV was insufficient. MUTZ-3 cells were infected for either 24 or 48 hours at varying MOI (0.1, 0.5, and 1). Cells were stained with 4G2-FITC in order to assess intracellular infection of MUTZ-3 cells. (A) MUTZ-3 cells were differentiated with 150 ng/mL of GM-CSF and 50 ng/mL of IL-4, for 7 days (n = 3). (B) MUTZ-3 cells were differentiated using cytokines, 100 ng/mL of GM-CSF, 20 ng/mL of IL-4, and 2.5 ng/mL TNFα, for 7 days (n = 1).

DISCUSSION

In this study, we first developed human primary DCs flavivirus infectious models to understand how viruses (including DENV, ZIKV, JEV and YFV) can infect human DCs and modify host cellular pathways leading to different disease development. We used DENV and ZIKV to bring additional knowledge for anti-viral/vaccine development. We also used vaccine strains, YFV17D and JEV SA14-14-2 to complement our models for DENV and ZIKV. Additionally, understanding how effective vaccine strains impact the host cells help to determine which pathway(s) could be important to target for an anti-viral or vaccine development. We demonstrated that moDCs are sensitive to DENV, ZIKV and JEV infection but not to YFV. In addition to the human primary DCs flavivirus infectious model development, we identified the genome-wide signaling networks in primary human DCs infected with DENV or ZIKV. Our transcriptomic profiles of pure populations of infected moDCs provide an accurate map of the human moDCs signaling response during DENV or ZIKV infection. By comparing the transcriptomes of DENV infected and ZIKV infected moDCs we have shown that even if these two viruses are genetically close they do not have the same impact on the host cells. ZIKV infection upregulate lipid metabolism while DENV infection modifies the inflammatory response.

We showed that our *in vitro* monocytes were differentiated into moDCs. Using these moDCs, we show that moDCs were sensitive to DENV-2 (UIS 353), ZIKV (SD001) and JEV (SA-14-14-2) infection. Other studies are in accordance to our results where they found that moDCs are sensitive to DENV3 (VN32/96 strain), ZIKV(PRVABC59) and JEV (Laos strain) (60). In this study they use different virus strains but the method of monocyte differentiation is identical to ours. The MOI used was identical for all viruses except ZIKV which they used a MOI of 1 while we

used a MOI of 0.5. Similarly, they reported a peak of infection at 24 hours for all three viruses, however, the percent of 4G2+ or E+ cells was lower in their study for DENV and ZIKV and similar to our results for JEV. Similarly, other studies show that moDCs are susceptible to DENV-2 infection. A different strain is used (DENV-2 New Guinea C strain) and they infect at multiple MOI (0.04, 0.1, 1, 10, 20) for 24 hours (61) . The percent of infection for 24 hours is similar but lower than our own results likely due to differences in strain or donor. Others have shown that moDCs are susceptible to infection by JEV SA14-14-2 and WT strains (62, 63). The vaccine strain has been used to infect moDCs that were differentiated in the same manner as described in this report, however CD1a expression was not recorded (62). YFV infectious models have been conducted by others. Gandini et al, have infected moDCs with YFV17D and show a peak of infection at 24 hours when infected at MOI 4. However, differentiation of monocytes to moDCs was conducted differently than in our model and CD1a expressing moDCs accounted for 56% of cells whereas in our model the percent of CD1a expression was higher than 90% (64). Since an alternative differentiation protocol was used and percent of cells expressing CD1a was reduced compared to our model, differences in infection reported could be cell dependent due to a non-homogenous population. Similarly, YFV Asibi and 17D strains have been shown to infect both macrophages and mature moDCs. In this study, cells were infected at a MOI 0.1. Peak infection for YFV17D and YFV Asibi strain was seen at 3- and 7-days post infection, respectively (65). Live-attenuated vaccine strain of JEV and YFV are expected to be less virulent and infectious which may account for our inability to infect YFV in our model. However, peak viral titer for YFV17D was higher than YFV Asibi strain (65) however this is cell type dependent.

In addition, it is interesting to note that infection seems to vary among cell type. In a previous study, our lab has shown that primary human macrophages were not sensitive to infection with two different ZIKV clinical isolates (SD001, FSS) (58). Primary human splenic macrophages

were sensitive to DENV after 48-hour infection at a MOI 5. However, B and T cells were not sensitive to DENV infection (66). Many factors can influence infection, among them are: the virus used (strain or serotype), or the cell type infected.

We found that DENV infection modulates the inflammatory response in moDCs. Similar results have been obtained in adults patients (67) and in children (68). An increase of inflammatory cytokines, IL-10 (67), IL-1β, IL-6 and IL-12 (68) have been described. In human hair follicle dermal papilla cells (HFDPC), DENV infection has been shown to activate the inflammatory response *in vitro*. In this study, HFDPCs were infected with a different and high MOI than our study and may not represent a biologically relevant model (MOI 10 and 50). This study used a different strain of DENV-2 (PL046) and also used DENV-1. DENV-1 and DENV-2 both increased the inflammatory response of HFDPCs by inducing expression of pro-inflammatory cytokines, IL-6, TNFα and IL-12b (69). Similarly, using a DENV-2 clinical isolate, it was shown that TNFα was significantly upregulated in non-transformed human fibroblasts (70). ZIKV has been shown to upregulate the inflammatory response in THP-1 macrophages (62). Similarly, our lab has previously shown that ZIKV upregulates the inflammatory response in monocyte derived human macrophages (58) . The inflammation response due to ZIKV infection may be cell type dependent. This activation is partly due to stress signals mediated by reactive oxygen species that function as a host cell defense against infection.

In our study, we found that ZIKV infection increase the lipid metabolism of moDCs. This result is in accordance with a patient study showing that the concentrations of several lipids species were increased in the serum of ZIKV infected patients compared to controls (71). Additionally, a mapping of host cell protein interactions with ZIKV genome reveals that the ZIKV C protein

interactome contains proteins involved in lipid storage and metabolism and C protein was found to colocalize with lipid droplets (72). In experiments conducted by our lab, after inhibition of FAS, a limiting enzyme implicated in fatty acid pathway, using C75, a decrease in ZIKV infection was observed in moDCs (unpublished data). Similarly, lipid homeostasis has been shown to be disturbed as a result of DENV infection in mosquito cells (73). After RNA-sequencing, we do not observe a modulation of lipid metabolism in DCs after DENV infection, therefore the results described by others are likely species and/or cell-type specific. Other flaviviruses have been shown to modulate the lipid metabolism such as HCV and WNV (74) (75). HCV infection leads to lipogenesis in infected cells. Additionally, HCV used cellular receptors implicated in lipid uptake (such as LDL-R or SR-B1) (76). HCV also used lipid droplets as a platform of its replication (77) and it is believed that viral production and secretion are dependent on very low-density lipoproteins (VLDL) (74). WNV infection in HeLa increases the amount of unsaturated phosphatidylcholine lipids (75). The alteration of lipid homeostasis in host cells creates a proper environment that is pivotal to the life cycle of these viruses.

We successfully developed a new flavivirus-DC infection model. In the process we identified important pathways modulated by ZIKV and DENV infection and showed that these pathways are virus dependent. This explains why even though these viruses are genetically close, they can have very different symptoms and disease progression. In our identification of the lipid pathways we may be able to target specific genes that allow us to develop a broad pan-flavivirus anti-viral treatment to, for example, target ZIKV and DENV simultaneously, since flaviviruses utilize the lipid metabolism pathway for replication. In the future, we aim to conduct RNA-sequencing on JEV for both wild-type and vaccine strains. With this information, we hope to

understand JEV infection in relation of other flaviviruses and elucidate what may make JEV vaccine strain unique in exhibiting a strong immunogenic response that is long lasting.

ACKNOWLEDGEMENTS

Figures 3-5 are coauthored with Dr. Aaron Carlin. The thesis author was the primary author. Figures 6-7 are coauthored with Dr. Emilie Branche. The thesis author was the primary author.

I would like to acknowledge Dr. Aaron Carlin and Dr. Emilie Branche for allowing me to use figures that they developed for this project.

APPENDIX

Supplementary tables with reagents and supplies

Cell culture

Item	Supplier	Catalog No.
MEM-α	Life technologies, GIBCO	12-561-072
Leibovitz L-15 Medium	Gibco	11-415-114
FBS	Gemini Bioproducts	100-106
Penicillin/Streptomycin (P/S)	Life technologies, GIBCO	15-140-163
HEPES	Life technologies, GIBCO	BP299100
0.25% Trypsin-EDTA, phenol red	Life technologies, GIBCO	25200056
50mL Conical tubes	Corning	14-432-22
15mL Conical tubes	Corning	14-959-70C
DMEM, no glucose	Gibco	11-966-025
T175 Vented	Thermo Scientific	12-556-011
T175 Non-vented	Thermo Scientific	12-556-014
T75 Vented	Thermo Scientific	12-556-010
6-Well Plate	Corning CoStar	3516

12-Well plates	Corning CoStar	3513
24-Well plates	Corning CoStar	3520
96 Well plate round bottom	Corning CoStar	3799
96-Well plate flat bottom	Corning CoStar	3596
Cell counter tube	Beckman Coulter Life Sciences	723908
PBS	Corning™	MT-21040-CM
C6/36	ATCC	
Vero cells	ATCC	
BHK-21 cells	ATCC	
MUTZ-3	DSMZ	ACC295

Virus concentration

100K or 50K column	Amicon	UFC910024
0.22 μm filter	MILLEX GV	SLGV033RS

PBMC isolation

Histopaque®-1077	M&P Biomedical	0219083780
10x PBS	Corning®	46-013-CM
Molecular grade water	Corning®	46-000-CM

Monocyte isolation and Differentiation verification

RPMI 1640 + glutaMAX	Gibco	61870-036
Pan Monocyte Isolation Kit, human	Miltenyi Biotech	130-096-537
Recombinant human GM-CSF (100 µg)	Pepro Tech	300-03
IL-4 (100 µg)	Pepro Tech	200-04
Tumor Necrosis Factor-α (TNF-α)	Pepro Tech	300-01A
LS columns	Miltenyi Biotech	130-042-401
Pre-separation filter (30 µm)	Miltenyi Biotech	130-041-407
Auto MACS rinsing solution	Miltenyi Biotech	130-091-222

Lipid experiments and Transfection using siRNA

StemFect RNA Transfection kit	Reprocell	00-0069
SMARTpool:ON-TARGETplus FASN siRNA	Dparmacon	L-003954-00-0005

SMARTpool:ON-TARGETplus SREBF1 siRNA	Dparmacon	L-006891-00-0005
SMARTpool:ON-TARGETplus SREBF2 siRNA	Dparmacon	L-009549-00-0005
ON-TARGETplus Non-targeting Pool	Dparmacon	D-001810-10-05
Quick-RNA microprep kit	Zymo Research	11-328M
Collection tubes (2 mL)	QIAGEN	1016810

cDNA and qRT-PCR

iSCRIPT cDNA synthesis kit	BIORAD	1708891
iTaq DNA polymerase	BIORAD	172520

FACS and Cell sort preparation

16% Paraformaldehyde	Electron microscopy sciences	15710-S
Saponin	Sigma Aldrich	47036-50G-F
BSA	Sigma-Aldrich	A3294-100G
40 µm filter	Fisher	08-771-1

EDTA (0.5 M), pH 8.0, RNase-free	Life technologies	AM9260G
Zombie violet fixable viability kit	BioLegend®	423113
PermWash concentrate	BD Biosciences	51-2091KZ
Compensation beads	Life Technologies	01-2222-42
Human FcX™True stain(Fc Receptor Blocking Solution)	BioLegend®	422302
Alexa Fluor 647 labeling kit	Invitrogen	A20186
BD cytofix/cytoperm	BD Bioscience	554722
APC anti-human CD1a Antibody	Biolegend®	300110
FITC anti-human CD14 Antibody	Biolegend®	301804
4G2 antibody	BIOXCELL	Lot#630816D1
Pierce FITC antibody labelling kit	Thermo Fischer Scientific	53027

RNA isolation

RNasin® Ribonuclease Inhibitors (Rnasine plus)	Promega	N2615

10X DNase I Buffer	Invitrogen	AM8179G
DNase	SIGMA	10104159001
TE Buffer	Invitrogen	12090-015
Total Nuclei Acid isolation kit	Ambion	AM1975
100% Absolute Ethanol	Fisher	BP2818500

FFA

CMC Sodium Salt, Medium viscosity	Sigma Aldrich	C9481-500G
Triton-X-100	Sigma Aldrich	9002-93-1
TruBlue	SERA CARE	5510-0030
Peroxidase AffiniPure Goat Anti-Mouse IgG, $F(ab')_2$ fragment specific	Jackson Immuno Research	115-035-072
10% Buffered Formalin Phosphate	FISCHER CHEMICAL	SF100-4

Forward and reverse primer sequences obtained from IDTDNA

hFASN

F- ACAGCGGGGAATGGGTACT

R- GACTGGTACAACGAGCGGAT

hSREBF1

F- ACAGTGACTTCCCTGGCCTAT

R- GCATGGACGGGTACATCTTCAA

hSREBF2

F- AACGGTCATTCACCCAGGTC

R- GGCTGAAGAATAGGAGTTGCC

hRPLPO

F- GTGTTCGACAATGGCAGCAT

R- GACACCCTCCAGGAAGCGA

REFERENCES

1. Griffiths MJ, Turtle L, Solomon T. 2014. Japanese encephalitis virus infection. *Handb Clin Neurol* 123: 561-76

2. Vicente-Santos A, Moreira-Soto A, Soto-Garita C, Chaverri LG, Chaves A, Drexler JF, Morales JA, Alfaro-Alarcon A, Rodriguez-Herrera B, Corrales-Aguilar E. 2017. Neotropical bats that co-habit with humans function as dead-end hosts for dengue virus. *PLoS Negl Trop Dis* 11: e0005537

3. Blitvich BJ, Firth AE. 2015. Insect-specific flaviviruses: a systematic review of their discovery, host range, mode of transmission, superinfection exclusion potential and genomic organization. *Viruses* 7: 1927-59

4. Souza-Neto JA, Powell JR, Bonizzoni M. 2019. Aedes aegypti vector competence studies: A review. *Infect Genet Evol* 67: 191-209

5. Heinz FX, Stiasny K. 2012. Flaviviruses and flavivirus vaccines. *Vaccine* 30: 4301-6

6. Byk LA, Gamarnik AV. 2016. Properties and Functions of the Dengue Virus Capsid Protein. *Annu Rev Virol* 3: 263-81

7. Roby JA, Setoh YX, Hall RA, Khromykh AA. 2015. Post-translational regulation and modifications of flavivirus structural proteins. *J Gen Virol* 96: 1551-69

8. Li L, Lok SM, Yu IM, Zhang Y, Kuhn RJ, Chen J, Rossmann MG. 2008. The flavivirus precursor membrane-envelope protein complex: structure and maturation. *Science* 319: 1830-4

9. Harrison SC. 2008. Viral membrane fusion. *Nat Struct Mol Biol* 15: 690-8

10. Chen S, Wu Z, Wang M, Cheng A. 2017. Innate Immune Evasion Mediated by Flaviviridae Non-Structural Proteins. *Viruses* 9

11. Lescar J, Soh S, Lee LT, Vasudevan SG, Kang C, Lim SP. 2018. The Dengue Virus Replication Complex: From RNA Replication to Protein-Protein Interactions to Evasion of Innate Immunity. *Adv Exp Med Biol* 1062: 115-29

12. Murray CL, Jones CT, Rice CM. 2008. Architects of assembly: roles of Flaviviridae non-structural proteins in virion morphogenesis. *Nat Rev Microbiol* 6: 699-708

13. Hackett BA, Cherry S. 2018. Flavivirus internalization is regulated by a size-dependent endocytic pathway. *Proc Natl Acad Sci U S A* 115: 4246-51

14. Apte-Sengupta S, Sirohi D, Kuhn RJ. 2014. Coupling of replication and assembly in flaviviruses. *Curr Opin Virol* 9: 134-42

15. Sirohi D, Kuhn RJ. 2017. Zika Virus Structure, Maturation, and Receptors. *J Infect Dis* 216: S935-S44

16. Mustafa MS, Rasotgi V, Jain S, Gupta V. 2015. Discovery of fifth serotype of dengue virus (DENV-5): A new public health dilemma in dengue control. *Med J Armed Forces India* 71: 67-70

17. Rush B. 1786. Result of Some Observations Made by Benjamin Rush, M. D. Professor of Chemistry in the University of Philadelphia, during His Attendance as Physician General of the Military Hospitals of the United States in the Late War. *Lond Med J* 7: 76-81

18. Brathwaite Dick O, San Martin JL, Montoya RH, del Diego J, Zambrano B, Dayan GH. 2012. The history of dengue outbreaks in the Americas. *Am J Trop Med Hyg* 87: 584-93

19. Bhatt S, Gething PW, Brady OJ, Messina JP, Farlow AW, Moyes CL, Drake JM, Brownstein JS, Hoen AG, Sankoh O, Myers MF, George DB, Jaenisch T, Wint GR, Simmons CP, Scott TW, Farrar JJ, Hay SI. 2013. The global distribution and burden of dengue. *Nature* 496: 504-7

20. Brady OJ, Gething PW, Bhatt S, Messina JP, Brownstein JS, Hoen AG, Moyes CL, Farlow AW, Scott TW, Hay SI. 2012. Refining the global spatial limits of dengue virus transmission by evidence-based consensus. *PLoS Negl Trop Dis* 6: e1760

21. H. OW. 2019. Dengue and Severe Dengue.

22. Fatima K, Syed NI. 2018. Dengvaxia controversy: impact on vaccine hesitancy. *J Glob Health* 8: 010312

23. Schmid MA, Diamond MS, Harris E. 2014. Dendritic cells in dengue virus infection: targets of virus replication and mediators of immunity. *Front Immunol* 5: 647

24. Guzman MG, Vazquez S. 2010. The complexity of antibody-dependent enhancement of dengue virus infection. *Viruses* 2: 2649-62

25. Kliks SC, Nimmanitya S, Nisalak A, Burke DS. 1988. Evidence that maternal dengue antibodies are important in the development of dengue hemorrhagic fever in infants. *Am J Trop Med Hyg* 38: 411-9

26. Gardner CL, Ryman KD. 2010. Yellow fever: a reemerging threat. *Clin Lab Med* 30: 237-60

27. 2016. Dengue vaccine: WHO position paper - July 2016. *Wkly Epidemiol Rec* 91: 349-64

28. Low JG, Ooi EE, Vasudevan SG. 2017. Current Status of Dengue Therapeutics Research and Development. *J Infect Dis* 215: S96-S102

29. Wikan N, Smith DR. 2016. Zika virus: history of a newly emerging arbovirus. *Lancet Infect Dis* 16: e119-e26

30. Musso D, Gubler DJ. 2016. Zika Virus. *Clin Microbiol Rev* 29: 487-524

31. Skraning S, Lindskog BV. 2017. *Tidsskr Nor Laegeforen* 137

32. Colon-Gonzalez FJ, Peres CA, Steiner Sao Bernardo C, Hunter PR, Lake IR. 2017. After the epidemic: Zika virus projections for Latin America and the Caribbean. *PLoS Negl Trop Dis* 11: e0006007

33. Barbi L, Coelho AVC, Alencar LCA, Crovella S. 2018. Prevalence of Guillain-Barre syndrome among Zika virus infected cases: a systematic review and meta-analysis. *Braz J Infect Dis* 22: 137-41

34. Dimachkie MM, Barohn RJ. 2013. Guillain-barre syndrome. *Curr Treat Options Neurol* 15: 338-49

35. Wheeler AC. 2018. Development of Infants With Congenital Zika Syndrome: What Do We Know and What Can We Expect? *Pediatrics* 141: S154-S60

36. Lee BY, Alfaro-Murillo JA, Parpia AS, Asti L, Wedlock PT, Hotez PJ, Galvani AP. 2017. The potential economic burden of Zika in the continental United States. *PLoS Negl Trop Dis* 11: e0005531

37. Yun SI, Lee YM. 2014. Japanese encephalitis: the virus and vaccines. *Hum Vaccin Immunother* 10: 263-79

38. Cardoso Jda C, de Almeida MA, dos Santos E, da Fonseca DF, Sallum MA, Noll CA, Monteiro HA, Cruz AC, Carvalho VL, Pinto EV, Castro FC, Nunes Neto JP, Segura MN, Vasconcelos PF. 2010. Yellow fever virus in Haemagogus

leucocelaenus and Aedes serratus mosquitoes, southern Brazil, 2008. *Emerg Infect Dis* 16: 1918-24

39. Daffis S, Kontermann RE, Korimbocus J, Zeller H, Klenk HD, Ter Meulen J. 2005. Antibody responses against wild-type yellow fever virus and the 17D vaccine strain: characterization with human monoclonal antibody fragments and neutralization escape variants. *Virology* 337: 262-72

40. Monath TP, Vasconcelos PF. 2015. Yellow fever. *J Clin Virol* 64: 160-73

41. Barba-Spaeth G, Longman RS, Albert ML, Rice CM. 2005. Live attenuated yellow fever 17D infects human DCs and allows for presentation of endogenous and recombinant T cell epitopes. *J Exp Med* 202: 1179-84

42. Shearer FM, Longbottom J, Browne AJ, Pigott DM, Brady OJ, Kraemer MUG, Marinho F, Yactayo S, de Araujo VEM, da Nobrega AA, Fullman N, Ray SE, Mosser JF, Stanaway JD, Lim SS, Reiner RC, Jr., Moyes CL, Hay SI, Golding N. 2018. Existing and potential infection risk zones of yellow fever worldwide: a modelling analysis. *Lancet Glob Health* 6: e270-e8

43. H. OW. Yellow Fever.

44. Monath TP. 2012. Review of the risks and benefits of yellow fever vaccination including some new analyses. *Expert Rev Vaccines* 11: 427-48

45. Erlanger TE, Weiss S, Keiser J, Utzinger J, Wiedenmayer K. 2009. Past, present, and future of Japanese encephalitis. *Emerg Infect Dis* 15: 1-7

46. Campbell GL, Hills SL, Fischer M, Jacobson JA, Hoke CH, Hombach JM, Marfin AA, Solomon T, Tsai TF, Tsu VD, Ginsburg AS. 2011. Estimated global incidence of Japanese encephalitis: a systematic review. *Bull World Health Organ* 89: 766-74, 74A-74E

47. Wang P, Li M, Lu W, Zhang D, Hu Q, Liu Y. 2017. DC-SIGN promotes Japanese encephalitis virus transmission from dendritic cells to T cells via virological synapses. *Virol Sin* 32: 495-502

48. Guzman MG, Harris E. 2015. Dengue. *Lancet* 385: 453-65

49. Steinman RM, Hemmi H. 2006. Dendritic cells: translating innate to adaptive immunity. *Curr Top Microbiol Immunol* 311: 17-58

50. Musumeci A, Lutz K, Winheim E, Krug AB. 2019. What Makes a pDC: Recent Advances in Understanding Plasmacytoid DC Development and Heterogeneity. *Front Immunol* 10: 1222

51. Liu K, Nussenzweig MC. 2010. Origin and development of dendritic cells. *Immunol Rev* 234: 45-54

52. Posch W, Lass-Florl C, Wilflingseder D. 2016. Generation of Human Monocyte-derived Dendritic Cells from Whole Blood. *J Vis Exp*

53. Mahiddine K, Mallavialle A, Bziouech H, Larbret F, Bernard A, Bernard G. 2016. CD99 isoforms regulate CD1a expression in human monocyte-derived DCs through ATF-2/CREB-1 phosphorylation. *Eur J Immunol* 46: 1460-71

54. Santegoets SJ, van den Eertwegh AJ, van de Loosdrecht AA, Scheper RJ, de Gruijl TD. 2008. Human dendritic cell line models for DC differentiation and clinical DC vaccination studies. *J Leukoc Biol* 84: 1364-73

55. Lundberg K, Albrekt AS, Nelissen I, Santegoets S, de Gruijl TD, Gibbs S, Lindstedt M. 2013. Transcriptional profiling of human dendritic cell populations and models--unique profiles of in vitro dendritic cells and implications on functionality and applicability. *PLoS One* 8: e52875

56. Kosten IJ, Spiekstra SW, de Gruijl TD, Gibbs S. 2015. MUTZ-3 derived Langerhans cells in human skin equivalents show differential migration and phenotypic plasticity after allergen or irritant exposure. *Toxicol Appl Pharmacol* 287: 35-42

57. Masterson AJ, Sombroek CC, De Gruijl TD, Graus YM, van der Vliet HJ, Lougheed SM, van den Eertwegh AJ, Pinedo HM, Scheper RJ. 2002. MUTZ-3, a human cell line model for the cytokine-induced differentiation of dendritic cells from CD34+ precursors. *Blood* 100: 701-3

58. Carlin AF, Vizcarra EA, Branche E, Viramontes KM, Suarez-Amaran L, Ley K, Heinz S, Benner C, Shresta S, Glass CK. 2018. Deconvolution of pro- and antiviral genomic responses in Zika virus-infected and bystander macrophages. *Proc Natl Acad Sci U S A* 115: E9172-E81

59. Larsson K, Lindstedt M, Borrebaeck CA. 2006. Functional and transcriptional profiling of MUTZ-3, a myeloid cell line acting as a model for dendritic cells. *Immunology* 117: 156-66

60. Garcia-Nicolas O, Lewandowska M, Ricklin ME, Summerfield A. 2019. Monocyte-Derived Dendritic Cells as Model to Evaluate Species Tropism of Mosquito-Borne Flaviviruses. *Front Cell Infect Microbiol* 9: 5

61. Olagnier D, Peri S, Steel C, van Montfoort N, Chiang C, Beljanski V, Slifker M, He Z, Nichols CN, Lin R, Balachandran S, Hiscott J. 2014. Cellular oxidative stress response controls the antiviral and apoptotic programs in dengue virus-infected dendritic cells. *PLoS Pathog* 10: e1004566

62. Wang W, Li G, De W, Luo Z, Pan P, Tian M, Wang Y, Xiao F, Li A, Wu K, Liu X, Rao L, Liu F, Liu Y, Wu J. 2018. Zika virus infection induces host inflammatory responses by facilitating NLRP3 inflammasome assembly and interleukin-1beta secretion. *Nat Commun* 9: 106

63. Manh DH, Mizukami S, Dumre SP, Raekiansyah M, Senju S, Nishimura Y, Karbwang J, Huy NT, Morita K, Hirayama K. 2018. iPS cell serves as a source of dendritic cells for in vitro dengue virus infection model. *J Gen Virol* 99: 1239-47

64. Gandini M, Reis SR, Torrentes-Carvalho A, Azeredo EL, Freire Mda S, Galler R, Kubelka CF. 2011. Dengue-2 and yellow fever 17DD viruses infect human dendritic cells, resulting in an induction of activation markers, cytokines and chemokines and secretion of different TNF-alpha and IFN-alpha profiles. *Mem Inst Oswaldo Cruz* 106: 594-605

65. Cong Y, McArthur MA, Cohen M, Jahrling PB, Janosko KB, Josleyn N, Kang K, Zhang T, Holbrook MR. 2016. Characterization of Yellow Fever Virus Infection of Human and Non-human Primate Antigen Presenting Cells and Their Interaction with CD4+ T Cells. *PLoS Negl Trop Dis* 10: e0004709

66. Blackley S, Kou Z, Chen H, Quinn M, Rose RC, Schlesinger JJ, Coppage M, Jin X. 2007. Primary human splenic macrophages, but not T or B cells, are the principal target cells for dengue virus infection in vitro. *J Virol* 81: 13325-34

67. Tsai TT, Chuang YJ, Lin YS, Wan SW, Chen CL, Lin CF. 2013. An emerging role for the anti-inflammatory cytokine interleukin-10 in dengue virus infection. *J Biomed Sci* 20: 40

68. Sprokholt J, Helgers LC, Geijtenbeek TB. 2017. Innate immune receptors drive dengue virus immune activation and disease. *Future Virol* 13: 287-305

69. Wei KC, Huang MS, Chang TH. 2018. Dengue Virus Infects Primary Human Hair Follicle Dermal Papilla Cells. *Front Cell Infect Microbiol* 8: 268

70. Bustos-Arriaga J, Garcia-Machorro J, Leon-Juarez M, Garcia-Cordero J, Santos-Argumedo L, Flores-Romo L, Mendez-Cruz AR, Juarez-Delgado FJ, Cedillo-Barron L. 2011. Activation of the innate immune response against DENV in normal non-transformed human fibroblasts. *PLoS Negl Trop Dis* 5: e1420

71. Queiroz A, Pinto IFD, Lima M, Giovanetti M, de Jesus JG, Xavier J, Barreto FK, Canuto GAB, do Amaral HR, de Filippis AMB, Mascarenhas DL, Falcao MB, Santos NP, Azevedo VAC, Yoshinaga MY, Miyamoto S, Alcantara LCJ. 2019. Lipidomic Analysis Reveals Serum Alteration of Plasmalogens in Patients Infected With ZIKA Virus. *Front Microbiol* 10: 753

72. Coyaud E, Ranadheera C, Cheng D, Goncalves J, Dyakov BJA, Laurent EMN, St-Germain J, Pelletier L, Gingras AC, Brumell JH, Kim PK, Safronetz D, Raught B. 2018. Global Interactomics Uncovers Extensive Organellar Targeting by Zika Virus. *Mol Cell Proteomics* 17: 2242-55

73. Perera R, Riley C, Isaac G, Hopf-Jannasch AS, Moore RJ, Weitz KW, Pasa-Tolic L, Metz TO, Adamec J, Kuhn RJ. 2012. Dengue virus infection perturbs lipid homeostasis in infected mosquito cells. *PLoS Pathog* 8: e1002584

74. Syed GH, Amako Y, Siddiqui A. 2010. Hepatitis C virus hijacks host lipid metabolism. *Trends Endocrinol Metab* 21: 33-40

75. Martin-Acebes MA, Merino-Ramos T, Blazquez AB, Casas J, Escribano-Romero E, Sobrino F, Saiz JC. 2014. The composition of West Nile virus lipid envelope unveils a role of sphingolipid metabolism in flavivirus biogenesis. *J Virol* 88: 12041-54

76. Lindenbach BD, Rice CM. 2013. The ins and outs of hepatitis C virus entry and assembly. *Nat Rev Microbiol* 11: 688-700

77. Ogawa K, Hishiki T, Shimizu Y, Funami K, Sugiyama K, Miyanari Y, Shimotohno K. 2009. Hepatitis C virus utilizes lipid droplet for production of infectious virus. *Proc Jpn Acad Ser B Phys Biol Sci* 85: 217-28